Few-Layer MoS_2: A Promising Layered Semiconductor

Rudren Ganatra and Qing Zhang*

NOVITAS, Nanoelectronics Centre of Excellence, School of Electrical and Electronic Engineering, Nanyang Technological University, 639798 Singapore

ABSTRACT Due to the recent expanding interest in two-dimensional layered materials, molybdenum disulfide (MoS_2) has been receiving much research attention. Having an ultrathin layered structure and an appreciable direct band gap of 1.9 eV in the monolayer regime, few-layer MoS_2 has good potential applications in nanoelectronics, optoelectronics, and flexible devices. In addition, the capability of controlling spin and valley degrees of freedom makes it a promising material for spintronic and valleytronic devices. In this review, we attempt to provide an overview of the research relevant to the structural and physical properties, fabrication methods, and electronic devices of few-layer MoS_2. Recent developments and advances in studying the material are highlighted.

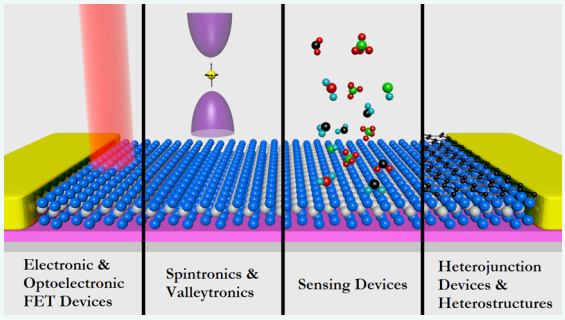

KEYWORDS: two-dimensional materials · molybdenum disulfide · transition metal dichalcogenides · 2D · nanosheets

The ability to obtain single-layer graphene[1,2] opened up new possibilities and research into the physics of two-dimensional materials. The availability of advanced equipment and tools and a growing understanding of atomically thick layered materials have led to a burgeoning research interest into a whole new range of 2D materials such as transition metal dichalcogenides (TMDCs), topological insulators, *etc*. TMDCs are MX_2-type compounds where M is a transition element from groups IV, V, and VI of the periodic table and X represents the chalcogen species S, Se, and Te.[3−5] TMDCs can be semiconductors, semimetals/metals, or even superconductors. The presence of unsaturated d-orbitals contributed by transition metals to the material's band structure introduces a multitude of interesting properties such as charge density waves, magnetism, and superconductivity that make TMDCs an appealing focus for research.[3−7] The controlled filling of such d-orbitals using methods such as intercalation further facilitates engineering the material properties of band structure, magnetism, conductivity, and superconductivity.[3,4,6,8−10] Two-dimensional TMDCs have strong molecular intralayer bonds but weak interlayer bonds, giving rise to their layered structure and consequent anisotropic properties. MoS_2 has been one of the most studied TMDCs due to its availability in nature as molybdenite. It has been studied since the 1960s in the fields of dry lubrication,[11−16] catalysis,[17−21] photovoltaics,[22−26] and batteries.[27−33] It is only very recently that few-layer MoS_2 has attracted a lot of attention for its promising semiconducting characteristics and potential applications in nanoelectronics and optoelectronics. This review is an attempt to systematically categorize and summarize the research activities in MoS_2-based electronics and optoelectronics.

Material Structure and Physics. *Crystal Structure.* The basic crystal structure of molybdenum disulfide has been studied for more than 5 decades.[2,34−50] It is only recently that it has been under study from electronic and optoelectronic perspectives.[50] MoS_2 has a two-dimensional layered structure similar to graphene, with the individual layers stacked upon each other to form the bulk (see Figure 1). Each 2D crystal layer is about 0.65 nm thick. These layers are held together by weak van der Waals forces. This makes it possible to obtain single- to few-layer crystal flakes using the scotch tape mechanical exfoliation method, which was employed to fabricate the first graphene flake[2] and shall be addressed later in this review.[2,34,35,39,45,46,50−52]

* Address correspondence to eqzhang@ntu.edu.sg.

Received for review November 16, 2013 and accepted March 24, 2014.

Published online March 24, 2014
10.1021/nn405938z

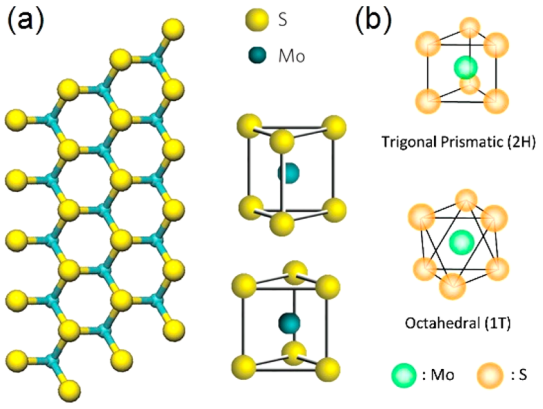

Figure 1. Crystal structure of MoS_2. (a) Top view of monolayer hexagonal crystal structure of MoS_2. (b) Trigonal prismatic (2H) and octahedral (1T) unit cell structures. Panel a reprinted by permission from Macmillan Publishers Ltd: Nature Photonics, ref 53, copyright 2012. Panel b reproduced from ref 54. Copyright 2011 American Chemical Society.

Each 2D crystal layer of MoS_2 has a plane of hexagonally arranged molybdenum atoms sandwiched between two planes of hexagonally arranged sulfur atoms, with the covalently bonded S−Mo−S atoms in a trigonal prismatic arrangement forming a hexagonal crystal structure. The most commonly found crystal symmetry configurations for MoS_2 are hexagonal and octahedral structures. The former is semiconducting, and the latter is metallic. The former was discovered much earlier than the latter.[51] In theory, the former is more stable than the latter.[55] The Mo−S bond length is 2.4 Å, the crystal lattice constant is 3.2 Å, and the distance between the upper and lower sulfur atoms is 3.1 Å.[55,56]

MoS_2 has been shown to possess very high mechanical strength and has a higher Young's modulus than that of steel.[57−60] A monolayer of MoS_2 is marginally stronger than the bulk crystal.[60] MoS_2 crystal layers can be deformed by up to 11% without fracture[57,60] and be bent to a curvature of the radius of 0.75 mm without losing their electronic properties.[61] These merits make MoS_2 a promising material for flexible electronics. MoS_2 has piezoelectric properties, and it can be utilized for sensitive mechanical transducers.[62] MoS_2-based nanomechanical resonators could function in the HF (high-frequency, 3−30 MHz) and VHF (very high frequency, 30−300 MHz) bands with good performance[63,64] and showed a very high figure of merit (a measure of device performance given by product of resonant frequency and *Q* factor) of about 2×10^{10} Hz at room temperature.[64]

Bulk MoS_2 belongs to the D_{6h} crystal structure space group, while monolayer MoS_2 belongs to the D_{3h} space group.[55,56,65−67] D_{6h} possesses inversion symmetry, while D_{3h} lacks inversion symmetry. Optical second harmonic microscopy is a very useful tool in characterizing mono- to trilayer MoS_2 and determining crystal orientation, crystal domain, size, and layer stacking.[68,69] Optical second harmonic studies show retention of the bulk lattice symmetry in few-layer MoS_2. Few-layer MoS_2 with an even number of layers retains inversion symmetry, but odd layered MoS_2 does not.[70] This has been confirmed by strong enhancement of optical second harmonic intensity in the odd layered samples.

Raman Studies. Raman spectroscopy is very popularly used to study crystal quality as well as accurately identify the layer number of MoS_2 flakes. MoS_2 has four Raman-active modes (E_{1g}, E_{2g}^1, A_{1g}, and E_{2g}^2) and two IR-active modes (A_{2u} and E_{1u}) (see Figure 2a).[56,65−67] The E_{2g}^1 is an in-plane mode resulting from the opposite vibration of two S atoms with respect to the Mo between them, while the A_{1g} mode is attributed to the out-of-plane vibration of only S atoms in opposite directions. From monolayer to bulk, the E_{2g}^1 mode undergoes a red shift while the A_{1g} mode undergoes a blue shift (see Figure 2c).[49,66,71] The E_{2g}^1 mode is believed to be affected by the long-range interlayer Coulombic interaction between molybdenum atoms with increasing layer number due to the increase in the dielectric tensor. The A_{1g} mode on the other hand is less affected by interlayer interactions.[72] The A_{1g} mode is very sensitive to adsorbates on the MoS_2 surface[73] and electron doping.[74] Due to stronger electron−phonon coupling of the A_{1g} mode, it shows a red shift and an increase in the peak width with increasing doping level. The frequency or frequency-shift difference between these two modes on the Raman spectrum can be used to determine the layer number of few-layer flakes.[49] There also exist low-frequency interlayer breathing (B_{2g}^2) and shear (E_{2g}^2) modes (see Figure 2b,d,e), which are functions of the layer number and can be used to examine the structural properties of few-layer MoS_2 flakes and determine layer number.[65,75,76] The shear mode E_{2g}^2 is found to undergo a blue shift on increasing the layer number, while the opposite is seen for the breathing mode B_{2g}^2. Both modes vanish for single-layer MoS_2, being consistent with the understanding that these two modes are a result of interlayer interaction. An increase in temperature causes an appreciable red shift of E_{2g}^1 and A_{1g}.[67,77,78] The intensity and full width at half-maximum (fwhm) values for these peaks are also greater at higher temperatures. E_{2g}^1 is also sensitive to applied strain and shows a red shift with increasing strain.[79]

While there are multiple interesting factors affecting each of the Raman modes observed in MoS_2, it would be very difficult to separate all the factors affecting the spectrum. Even through comparison with known observational values, there may be other factors affecting the Raman spectrum that have not been studied yet about which conclusions cannot be made without losing out on data and inferential correctness.

Band Structure. MoS_2 belongs to a unique class of layered materials[47,55,81] known as transition metal dichalcogenides whose band gaps vary with the number of layers. Bulk MoS_2 has an indirect band gap of 1.29 eV (see Figure 3a,b).[47,50,55] The band structure and band

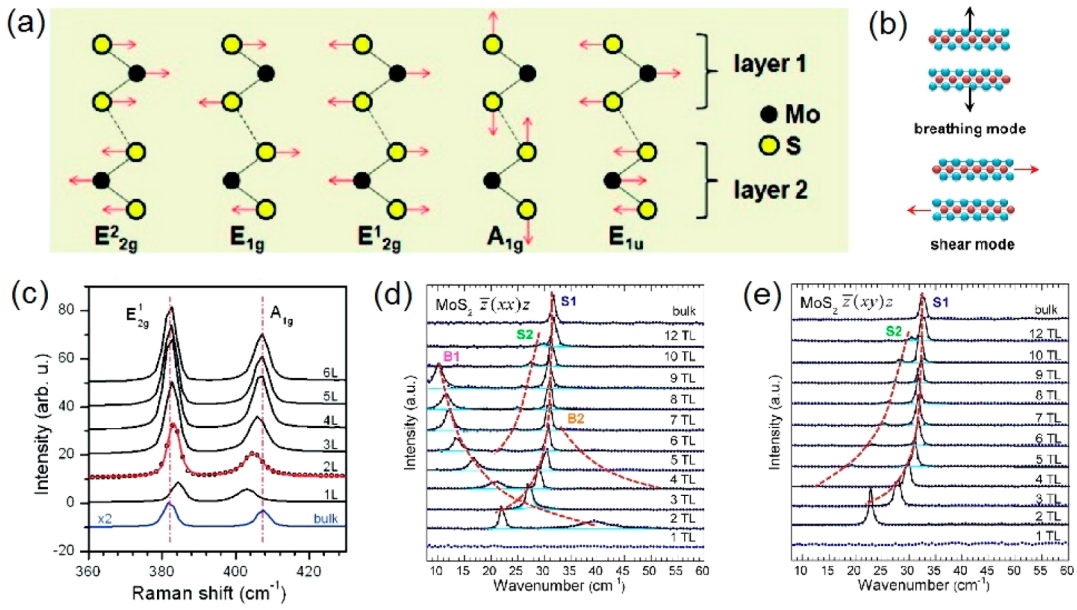

Figure 2. Raman and IR-active phonons. (a) Illustrations of the four Raman-active phonon modes (E_{1g}, $E_{2g}{}^1$, A_{1g}, and $E_{2g}{}^2$) and one IR-active phonon mode (E_{1u}) and their interlayer interactions. (b) Illustrations of the interlayer breathing and shear modes. (c) $E_{2g}{}^1$ and A_{1g} Raman peaks in few-layer flakes. (d,e) Evolution of low-frequency spectra with increasing layer number of the interlayer breathing (B1 and B2) and shear (S1 and S2) modes using (d) the (*xx*)*z* polarization configuration and (e) the (*xy*)*z* polarization configuration. Panels a and c reprinted from ref 49. Copyright 2010 American Chemical Society. Panels b, d, and e reprinted from ref 65. Copyright 2013 American Chemical Society.

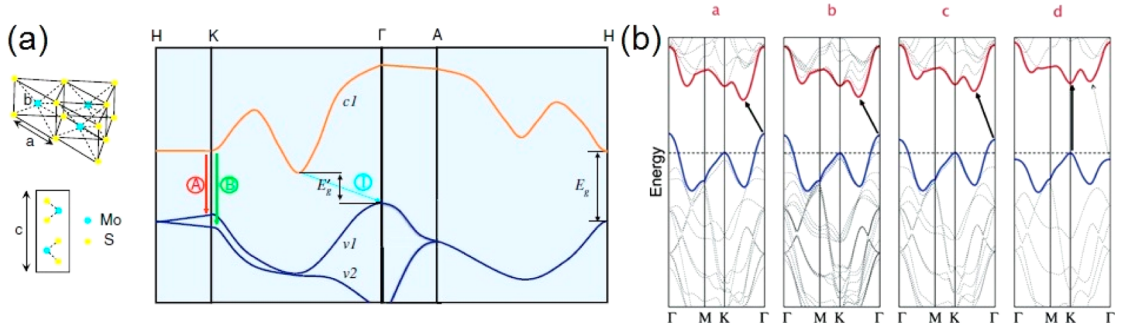

Figure 3. Band structure of MoS_2 (a) showing the direct and indirect band gap, as well as the A and B excitons. (b) Transition of the band structure of MoS_2 from indirect to direct band gap (a → d). Panel a reprinted with permission from ref 50. Copyright 2010 American Physical Society. Panel b reprinted from ref 80. Copyright 2010 American Chemical Society.

gap of MoS_2 are strongly affected by quantum confinement owing to its ultrathin 2D crystal structure.[50,54,82] The valence band maximum is located at the Γ point, while the conduction band minimum is located almost halfway along the Γ−K direction, which constitutes the indirect band gap transition.[50,83,84] With the layer number decreasing, the lowest band in the conduction band moves upward, increasing the overall band gap. As the conduction band states at the K point are mainly due to the d-orbitals of the molybdenum atoms and are relatively unaffected by interlayer interactions, the direct band gap at the K point only increases by about 0.05−0.1 eV (see Figure 3b).[81,84] The states near the Γ point on the conduction band are due to hybridization between p_z-orbitals of sulfur atoms and the d-orbitals of molybdenum atoms and are affected by interlayer interactions. Thus the bands at Γ are more affected by a decrease in layer number.[80,81] In the monolayer, the indirect transition gap is larger than the direct transition gap, and the smallest band gap is thus the direct band gap at K point of about 1.9 eV. This transition from an indirect to a direct band gap semiconductor is very interesting and reflects interlayer interaction, quantum confinement, and long-range Coulomb effects.[47,50,55,80,83−85] Substrate interaction is also predicted to have a pronounced effect on the properties of few-layer MoS_2.[83] Due to the indirect to direct band gap transition observed in few-layer MoS_2 along with further band structure variations as a function of layer number, band calculations and material physics[83,84,86−94] are now receiving more attention as this phenomenon is quite unique from previously known materials and provides a whole new host of physics and applications.

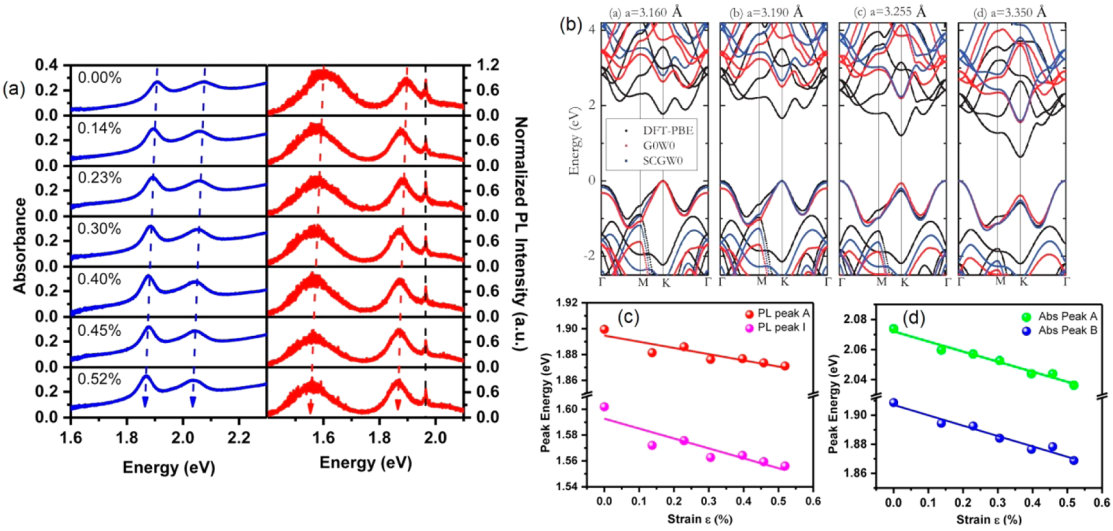

Figure 4. Variation of band structure properties with strain. (a,c,d) Shift of absorbance and photoluminescence peaks with application of uniaxial tensile strain. (b) Evolution of the band structure of monolayer MoS_2 under various values of biaxial strain and consequent lattice constants as measured using different calculation models (DFT-PBE, G0W0, SCGW0). Panels a, c, and d reprinted from ref 128. Copyright 2013 American Chemical Society. Panel b reprinted with permission from ref 124. Copyright 2013 American Physical Society.

Carrier Physics. The effective mass for electrons at the K point is calculated to be $0.48m_e$,[95] which is much higher than that in graphene ($0.012m_e$).[96] Carrier mobility and the carrier scattering processes in MoS_2 are dominated by interactions with acoustic phonons at lower temperatures (<100 K) and optical phonons at higher temperatures.[35,95] Under the strong effect of optical phonons on the mobility of electrons in single-layer MoS_2, first-principle calculations predict a mobility drop from ~2450 cm^2/Vs in the acoustic phonon dominated low-temperature regime to ~400 cm^2/Vs at room temperature in the optical phonon dominated higher temperature regime.[95] Strong electron−phonon interactions have also been suggested to be the reason for superconductivity in MoS_2.[97−99] A recent study of the temperature dependence of the mobility shows two distinct regimes which border at 200 K.[100] Quenching of the less dominating homopolar mode by the use of high-κ dielectric oxides could increase the carrier mobility.[82,95,100] It is noted that the experimentally determined mobilities are significantly smaller than theoretically predicted values. The difference may be due to charge impurities. MoS_2 also displays the presence of graphene-like ripples which may have a negative effect on carrier mobility.[101] A vertical electric field exerted to few-layer MoS_2 is found to be an efficient method for band gap engineering.[89,102] The band gap of bilayer MoS_2 could be tuned to zero with an electric field of about 1.0−1.5 V/Å.[103]

Under optical pumping, a carrier lifetime of ~100 ± 10 ps, a carrier diffusion coefficient of 20 ± 10 cm^2/s, and a substantially higher mobility of 800 cm^2/Vs were achieved.[104] The higher mobility was attributed to the ambipolar nature of carrier diffusion due to optical injection where the electron−hole pairs move as an almost charge-neutral pair and are less susceptible to Coulomb scattering, which could be the origin of the strong degradation of carrier mobilities seen in MoS_2. Employment of high-κ dielectrics may provide charge screening by decreasing Coulomb scattering[82,95,100,105] and allow for greater carrier mobilities in MoS_2 devices. In addition, high-κ dielectrics are also predicted to decrease the monolayer band gap and exciton binding energy closer to those seen in bulk MoS_2.[90] Most MoS_2 field-effect transistors (FETs) are predominantly n-type,[82,106−116] while some are p-type[117,118] or ambipolar.[61,119−121] A recent *ab initio* study[122] suggested that substrates may play strong roles in the doping MoS_2 due to the presence of surface states, impurities, and defects that may be present on the substrate surface. Such a doping behavior cannot be attributed to the defects in MoS_2 itself as such defects could create deep states which do not have strong doping effects. The substrate-induced doping may also be an alternative way to dope MoS_2.

Band Structure Engineering. Band structure engineering methods are desired in order to tailor the electronic properties of few-layer MoS_2 for specific applications. The application of strain is a very straightforward method of band engineering in which the crystal structure dimensions are altered through the application of force across specific axes. Theoretical work[123] predicts a band gap reduction under uniaxial compressive strain across the *c*-axis of the crystal structure of MoS_2, with both the conduction band maximum as well as valence band minimum moving toward each other. Biaxial tensile strain on the other hand causes the conduction band minimum at the point of indirect band transition to move upward, while the conduction band at the K point moves downward with no shift seen in the valence band at the Γ point (see Figure 4b).

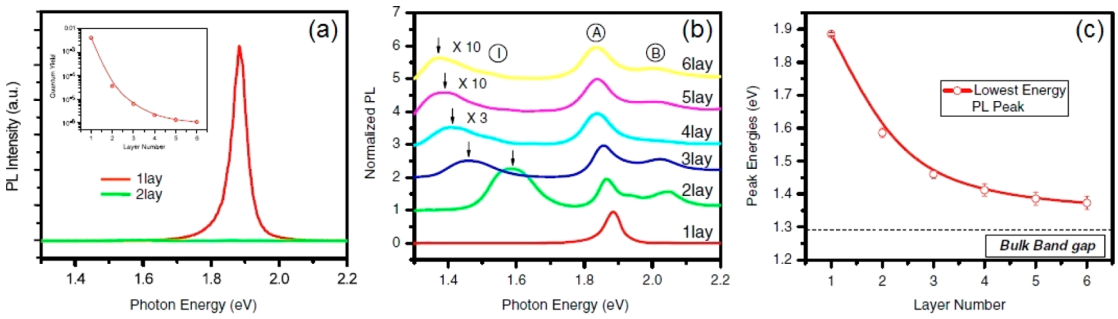

Figure 5. Optical characterization. (a) Photoluminescence spectra for monolayer and bilayer MoS_2. (b) Normalized photoluminescence spectra of MoS_2 with increasing number of layers, showing evolution of A and B excitons as well as the I peak of indirect transition. (c) Evolution of band gap with layer number of MoS_2. Reproduced with permission from ref 50. Copyright 2010 American Physical Society.

Band structure redesign under tensile strain is predicted to lower the electron effective mass and consequently improve electron mobility.[124] Applied strain could also cause band degeneracy which can be used for better spin-related properties and research in MoS_2.[123,125,126] Practical strain experiments[125,127−129] have shown results consistent with theoretical predictions, that is, up to ∼300 meV change in band gap per 1% applied strain.[127] A strain was found to cause a split in the E_{2g}^1 peak of the Raman spectrum coupled with a shift in the PL and absorbance spectrum (see Figure 4a,c,d) congruent with band gap change along with a large increase in PL intensity.[125,130] The impact of a strain on MoS_2 FET devices has also been theoretically modeled and predicted substantial improvement in the device performance.[126]

A material level method for band engineering is to grow alloys of MoS_2 and other TMDCs. As TMDCs have identical crystal structures with comparable bond lengths, it is theoretically feasible[131] to grow stable and miscible alloys of TMDCs including MoS_2, allowing precise band gap engineering over a much wider range and enabling the tuning of electronic and optical properties of the material. $Mo_{1-x}W_xS_2$ alloys were recently grown and studied.[132] The photoluminescence and Raman spectra showed the characteristics from both parent materials, and the band gap could be quite accurately tuned, suggesting a bowing effect like most other semiconductor alloys. Although much study is still required in such alloyed materials, this method shows promise in engineering tailored material properties. A first-principles-based study predicted band gap narrowing as well as transition to an indirect band gap of monolayer MoS_2 on using hexagonal boron nitride (h-BN) as a substrate due to surface-interaction-induced strain effects.[133] Monolayer MoS_2's band gap was predicted to decrease with increasing h-BN thickness until 5 layers of h-BN after which the band gap stabilizes.

Optical Physics. The direct optical band gap in single-layer MoS_2 opens up a whole new host of possibilities in optical properties and optoelectronic devices.[53,90,130,134−140] Photoluminescence studies show a very high quantum yield for monolayer MoS_2 and also affirm the optical transition band gap at around 1.9 eV (see Figure 5a).[50,54,80] While monolayer quantum yield was significantly higher than that of bulk (>10^4), the absolute value of quantum yield was still quite low (4×10^{-3}).[50] Photoluminescence (PL) tests along with Raman tests are frequently used in MoS_2 characterization and determination of the quality of MoS_2 growth, especially for monolayer growth quality and crystallinity.[54,80,107,108,111,116,141−144] Although the direct band gap in MoS_2 does exist even in the bulk structure, PL in the bulk is nonexistent due to excitonic absorption, but in the monolayer regime where the direct band gap is dominant, direct band radiative recombination becomes the principle method for excitonic recombination.[80] Direct as well as indirect exciton transition in mono-, bi-, and trilayer MoS_2 is found to be entirely a product of in-plane excitons[137] and may help in understanding exciton−phonon interactions. PL quantum yields for monolayer MoS_2 were found to be about 3 orders greater than that of multilayer MoS_2 due to radiative recombination across the direct band gap. A greater difference of 4 orders was obtained when monolayer MoS_2 was suspended.[50] Substrate contact and interface quality also has a substantial effect on PL tests and by extension may have effects on material performance.[145] Red shift of the PL spectra was observed with temperature increase, and this could be attributed to material expansion that induces a consequent increase in the in-plane lattice constant.[146] Excess charge transfer through adsorbed liquids or gases has been shown to suppress electrostatic screening, causing up to 2 orders of increase in the quantum yield of light emission from MoS_2.[147] Control of gas pressure provides accurate and reversible control of molecular adsorption on the MoS_2 surface at room temperature, thus controlling the amount of charge transfer and the resulting electrostatic screening. Few-layer MoS_2 is predicted to show a photothermoelectric effect with a very widely tunable Seebeck coefficient.[148]

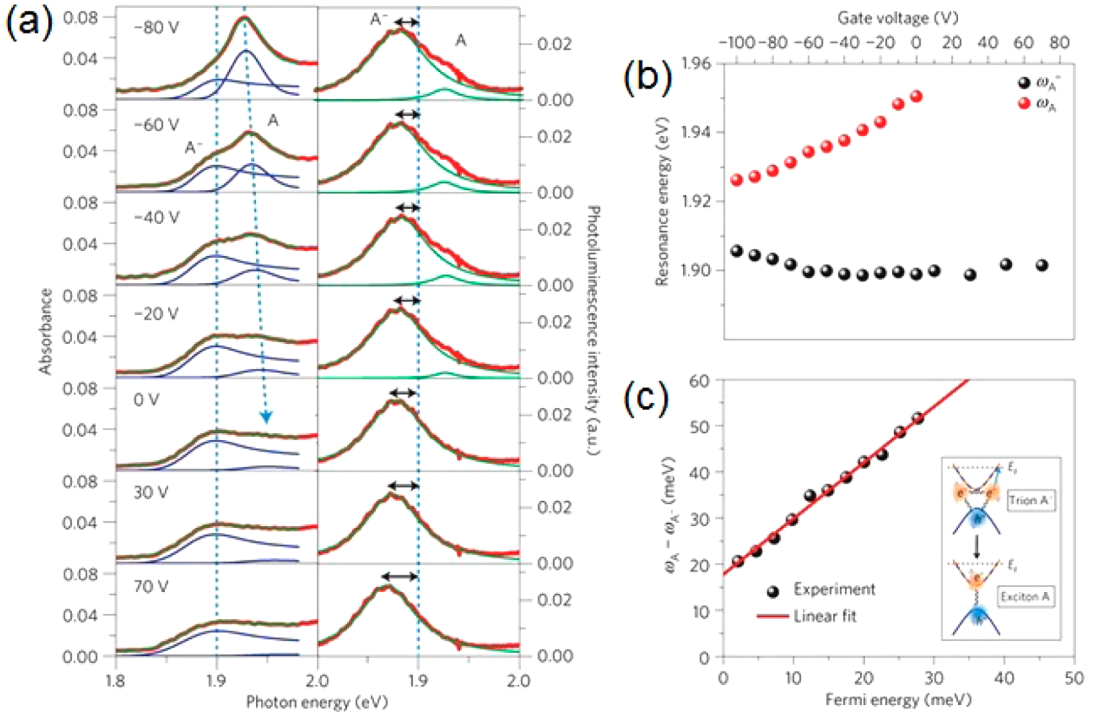

Figure 6. Trion behavior with gate-induced doping. (a) Absorbance and photoluminescence spectra of A excitons and A− trions with variation of indicated gate voltages. (b) Threshold energies of the trions ω_{A-} (black dots) and neutral exciton ω_A (red dots) plotted against gate voltage (above) and Fermi energy (below). (c) Plot of difference in energies between trions and excitons ($\omega_A - \omega_{A-}$) as a function of Fermi energy. Reprinted by permission from Macmillan Publishers Ltd: Nature Materials, ref 140, copyright 2012.

The photoluminescence spectra for MoS_2 show two exciton peaks (see Figure 5b) called exciton A (~1.92 eV) and B (~2.08 eV) at the K point[50,80] and are predicted to exist due to spin−orbit band splitting (145 meV[81]) in the valence band. This band splitting is the largest at the K point of the entire upper valence band, thus making two possible transitions available for excitons to the doubly degenerate conduction band.[80,81,149] These two excitons have high binding energies due to the low dielectric screening in monolayer MoS_2.[149] The introduction of excess electrons with the application of gate voltage shows a split in the absorption and photoluminescence spectra for exciton A (see Figure 6), found to be due to the existence of negative trions with high binding energies.[140] Trions were understood to be the product of interactions between an exciton and an electron (negative trion) or a hole (positive exciton) and were predicted to have lower binding energies as compared to excitons leading to the prediction of trions being stable mostly at lower temperatures.[150,151] The excess electrons present due to gate voltage application created favorable circumstances for the formation of trions.[140] While this experiment was mostly carried out at very low temperatures (10 K), the strong trion binding energies resulted in the observation of trion generation even at room temperatures, making this discovery quite significant. Large control was shown over the trion emission helicity by control of the polarization of incident light.[140] The ability to affect trion movement through the application of electric fields could be of great use in optoelectronics toward better control of such devices. The I peak (1.59 eV) shown in the PL spectrum could result from the indirect gap luminescence[50] and showed a blue shift with decreasing layer number consistent with the associated widening of the indirect band gap.

Band gap engineering through applied strain is very useful for tailoring the optical properties of materials, as well. As mentioned earlier, MoS_2 could be elastically deformed up to 11% without breaking the material.[57,60] A study by Feng *et al.*[152] took strain engineering a step further in proposing the use of strain on MoS_2 to create a broad-band optical funnel. The concept was to continuously vary strain across a sheet of monolayer MoS_2, causing a continuous variation of the optical band gap, allowing not only the capture of photons across a wide range of the solar spectrum but also guidance of the resulting generated excitons toward contacts. An implementation of such a structure could be a monolayer of MoS_2 suspended and anchored to form one contact over a circular hole while the center of the sheet over the hole is stretched downward and anchored at a point to another contact, literally taking the shape of a funnel (see Figure 7). The smoothly varied strain across the monolayer sheet from the edge of the hole to the stretched center of the monolayer to the contact below could result in

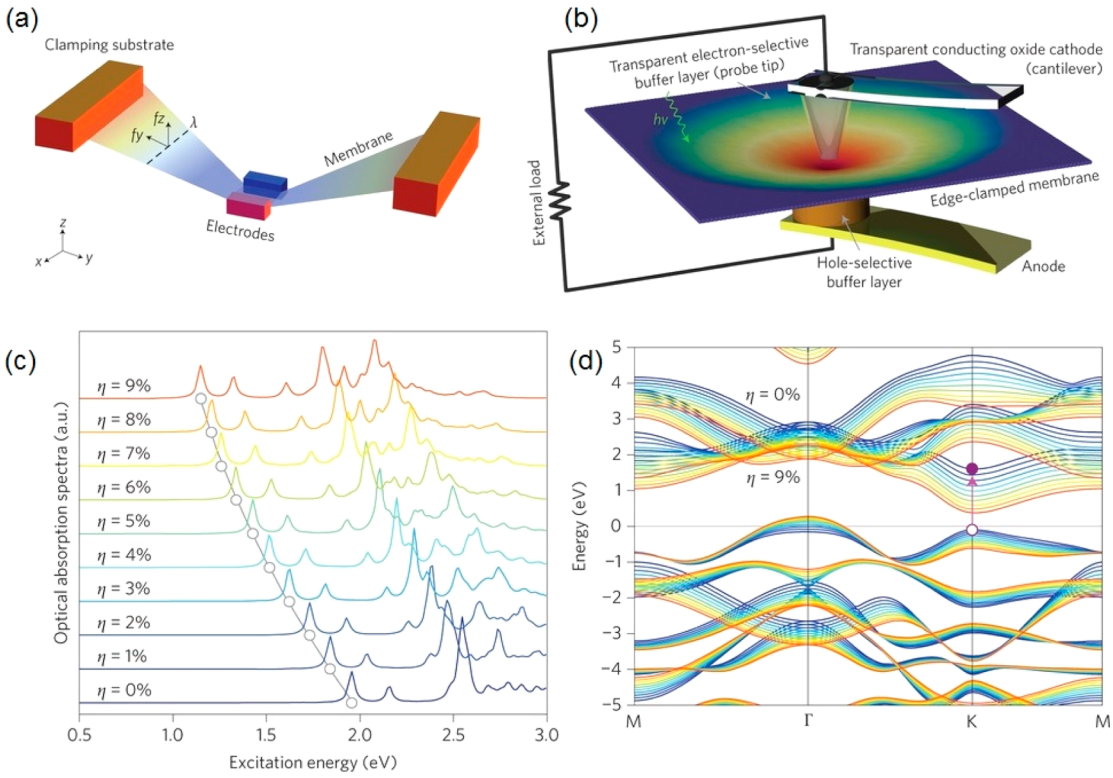

Figure 7. Strain-induced optical funnel. (a,b) Illustrations of the possible physical setups of a varying strain system. (c) Spectra of the band transition peaks with varying strain. (d) Variation of band structure with applied strain. Reprinted by permission from Macmillan Publishers Ltd: Nature Photonics, ref 152, copyright 2012.

a smooth narrowing of band gap. This is a very appealing concept and requires extensive practical experimentation to realize. A recent strain-engineered experiment[129] did show signs of a funnelling effect of excitons in MoS_2.

Spintronics and Valleytronics. Traditionally, a flow of electrons as current has been used in electronics for data transfer. Recently, more attention is being paid to other properties of electrons in order to hold or transmit data and information, like the spin and quantum state of an electron. Spintronics and valleytronics are two such fields of interest where a material's spin and valley quantum states are exploited for data and signal transfer.[154,155] Spintronics aims to utilize and control the quantized spin degrees of freedom of electrons for carrying data, while valleytronics takes advantage of materials having non-symmetric momentum valleys in their band structures with similar energy levels by polarizing electrons in a particular valley during conduction through the materials, thus controlling their valley degrees of freedom. Spin separation of carriers requires lifting of spin degeneracy on a material's energy bands. Spin−orbit interactions occur due to electric field asymmetries within a material through mainly two mechanisms depending on the source of such electric fields: surface electric fields (Rashba effect) and intracrystal electric fields (Dresselhaus effect).[156,157]

In monolayer MoS_2, the lack of inversion symmetry as well as spin−orbit interactions leads to a break in spin degeneracy along the Γ−K line of the conduction as well the valence bands, resulting in a band splitting of 148 eV.[156] Spin relaxation length was predicted to be quite large at about 0.4 μm at room temperature.[157] The band structure of monolayer MoS_2 displays two valleys, K+ and −K (or K_), at the extreme corners of the first Brillouin zone (see Figure 8a).[158,159] The broken inversion symmetry in monolayer MoS_2 also causes valley Hall effect where carriers flow into opposite transverse edges upon application of an in-plane electric field.[53,153,160] The nondegenerate spin energy bands coupled with time reversal symmetry of the monolayer MoS_2 crystal crystal pointed to coupling of spin and valley states in MoS_2, resulting in valley-dependent optical polarization selection for individual valleys.[156,159] Time reversal symmetry implies opposite spin-splitting in each valley energy momentum valley.[158,159] It can thus be understood that a particular valley would correspond to optical selection rules of a certain helicity as well as carriers of a fixed spin, while the opposite valley would correspond to opposite conditions, thus allowing control of carrier spin as well as carrier confinement within a specific valley with circularly polarized light (see Figure 9). Practical experiments observed that incidence of polarized light onto monolayer MoS_2 in turn emitted light of the same polarization, suggesting the presence of valley polarization (see Figure 8b).[53,153,161] Such valley polarization could be very well controlled.[158] The breaking of spin

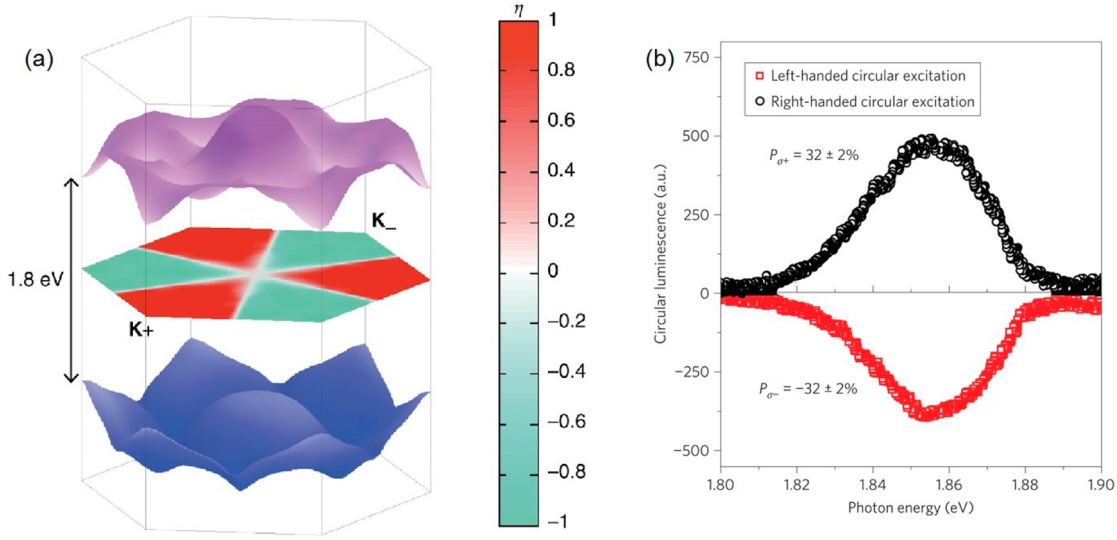

Figure 8. Valley polarization. (a) Illustration of the K (or K+, shown in red) and −K (or K_, shown in teal) valleys in the bottom of the conduction band (purple) and the top of the valence band (blue); η is the k-resolved degree of optical polarization between the top of the valence bands and the bottom of the conduction bands. (b) Data points of observed out-of-plane right (black) or left (red) polarized luminescence from monolayer MoS_2 when incident with correspondingly polarized light, where $P_{\sigma+}$ is the degree of right-circular polarization and $P_{\sigma-}$ is the degree of left-circular polarization. Panel a reprinted by permission from Macmillan Publishers Ltd: Nature Communications, ref 153, copyright 2012. Panel b reproduced with permission from ref 53. Copyright 2012 Nature Publishing Group.

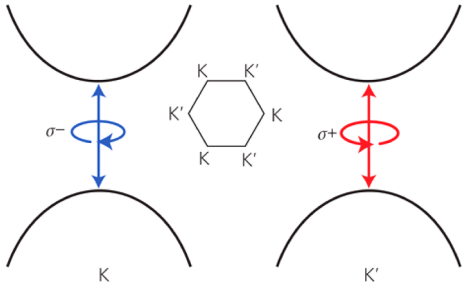

Figure 9. Spin and valley coupling. Illustration of the K (or K+) and K′ (or K_) coupled with left-circular (blue) and right-circular (red) spin-polarization. Reprinted by permission from Macmillan Publishers Ltd: Nature Nanotechnology, ref 53, copyright 2012.

degeneracy makes intervalley scattering forbidden and could result in long spin lifetimes in monolayer MoS_2. Hole spin lifetimes were already determined to be >1 ns.[158] The importance of spin and valley states was proven by performing the same study on bilayer MoS_2, where the inversion symmetry is retained, causing spin and valley states to be decoupled. It was found that the PL intensity was reduced by more than 20 times, and hole spin lifetime was 3 orders smaller than those observed in monolayer MoS_2. Spin and valley decoupling in this case allowed intervalley scattering to take place, leading to smaller spin lifetimes as well as a decreased degree of PL helicity.[158] The valley polarization was found to be strongly affected by temperature, which caused broadening in the energies of spin-up electrons much more than spin-down electrons.[162] Higher temperatures also lowered polarized emission from samples.[138] Recent experiments showed the control and tuning of circularly polarized photoluminescence from bilayer MoS_2 with the application of a gate voltage, attributed to the breaking of inversion symmetry in bilayer MoS_2 under the electric field.[163] Increased PL polarization in bilayer samples with increase in illumination source excitation power was also explained to be due to breaking of inversion symmetry possibly caused by an increase in temperature which may have consequently broken structural anisotropy.[53]

Magnetic Properties. MoS_2 flakes are diamagnetic[164] by nature but display ferromagnetism, as well,[164,165] which could be due to the magnetic moments from zigzag edges[164,165] as seen in MoS_2 nanoribbons[166] and from sulfur vacancies.[167] The ferromagnetism observed was enhanced as few-layer MoS_2 sheet size decreased[165] and was independent of layer coupling.[164] Magnetism can be artificially induced in few-layer MoS_2 through proton irradiation[168] and doping with certain atom species such as Mn.[169]

Fabrication and Growth. *Exfoliation.* Although the existence of layered bulk crystalline materials has been known for many years, scientists had believed that the single-layer crystalline forms of such materials would be too unstable for use or study.[2] Novoselov *et al.*[2] were among the first to use mechanical exfoliation or the "Scotch tape method" to obtain few- or even single-layer graphite, or graphene. Soon after that, other atomic thick 2D materials have been fabricated from layered materials such as MoS_2, boron nitride, and many more. In the mechanical exfoliation process, a small high-quality natural bulk MoS_2 crystal is adhered to a stretch of adhesive tape, repeatedly exfoliated followed by being adhered on a substrate.

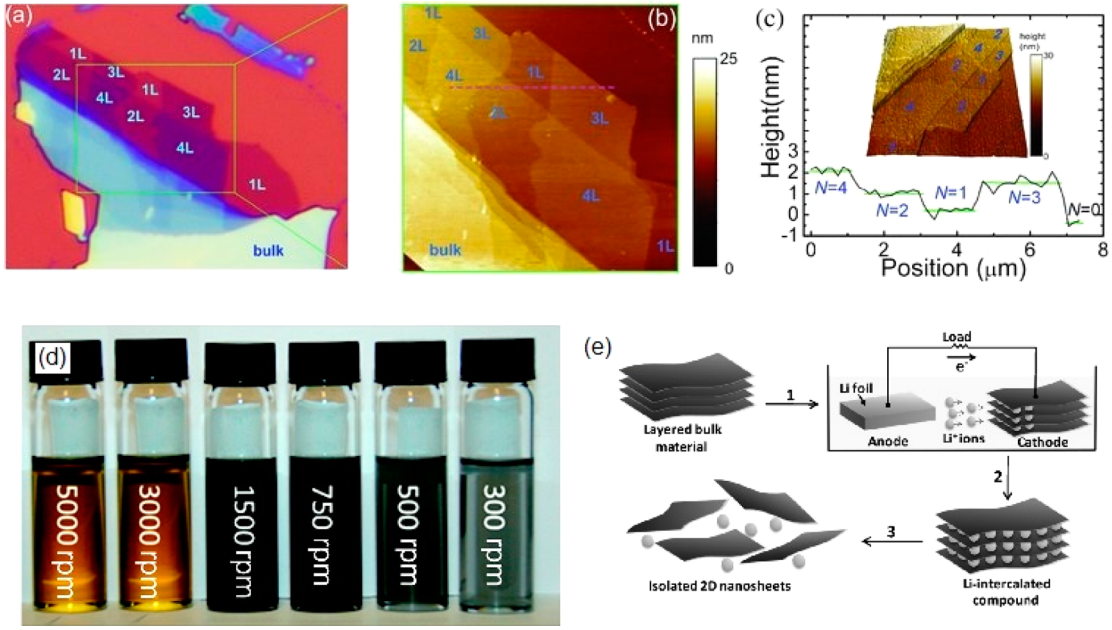

Figure 10. Exfoliation of MoS_2. (a) Optical and (b) AFM height image of multilayer sections of a MoS_2 flake on a 285 nm silicon oxide substrate. (c) Height profile of a MoS_2 flake measured along the dotted line in (b). (d) Chemically exfoliated MoS_2 flakes, roughly segregated according to flake size at different rpm through centrifugation. (e) Illustration of controlled lithiation and subsequent exfoliation using an electrochemical setup. Panels a−c reproduced with permission from ref 71. Copyright 2012 Wiley-VCH Verlag GmbH & Co. KGaA. Panel d reproduced from ref 178. Copyright 2012 American Chemical Society. Panel e reproduced with permission from ref 179. Copyright 2011 Wiley-VCH Verlag GmbH & Co. KGaA.

This causes ultrathin material layers to be left on the substrate.[2]

To observe the monolayer or few-layer MoS_2 flakes on the substrate, a specific thick dielectric-layer-coated substrate is needed as the exfoliated monolayer or few-layer MoS_2 must have an excellent optical contrast to be easily identified under an optical microscope.[2] Silicon oxide is the most commonly used substrate. The ideal silicon oxide thickness for the optical identification of single- to few-layer MoS_2 has been studied by several groups (see Figure 10a).[170−173] The 270−300 μm thick SiO_2 has been most commonly used for the purpose of direct observation.[82,100,113,120,163,174−177]

MoS_2 flakes obtained through mechanical exfoliation are usually preferred for research as they possess perfect crystalline structure and pristine quality. However, the yield of this process is extremely low. Most few-layer flakes obtained using this method range from a few micrometers to few tens of micrometers in size. A modified version of mechanical exfoliation, using wafer anodic bonding,[180] was reported to have a higher yield and better control over the number of layers. By placing a bulk crystalline MoS_2 on a piece Pyrex glass, contacting an anode to the MoS_2 crystal and a cathode to the back surface of the Pyrex glass, a voltage (200−1500 V) applied to the anode and cathode at 130−200 °C facilitated anodic bonding. Last, an adhesive tape was used to mechanically peel away the bonded crystal, leaving very thin flakes on the glass substrate.

Another class of exfoliation used to separate crystalline MoS_2 layers is so-called chemical exfoliation, which has been known much earlier than mechanical exfoliation.[40,181] Chemical exfoliation has recently gained huge interest due to the new physics and applications of layered materials. There are two basic approaches: ion intercalation and solvent-based exfoliation.

An ion intercalation method was first used in 1986 by Joensen *et al.*,[40] also referred to as the Morrison method. The ion intercalation method uses the concept of ion insertion in the gaps between the MoS_2 layers, widening the layer gaps. As lithium ions are very small, *n*-butyl lithium in hexane is a commonly used solution as a source of lithium ions. After Li ion intercalation, water is introduced and it vigorously reacts with the intercalated lithium ions to form hydrogen gas between the MoS_2 layers. The released hydrogen gas forces the MoS_2 layers apart, resulting in mostly single-layer sheets in the suspension. Methanol, ethanol, isopropyl alcohol, or rapid heating in vacuum at around 600 °C can also be used to release MoS_2 layers instead of water.[40] Some difficulties with this process are the relatively high temperatures required (100 °C) and lengthy reaction time (around 3 days). There is also little control over the extent of intercalation. A low level of intercalation results in a low yield of single-layer sheets, while excess intercalation causes decomposition of MoS_2 into metal nanoparticles along with the generation of Li_2S. Ion intercalation also causes MoS_2's crystalline structure to convert from 2H (hexagonal, semiconducting) to 1T-MoS_2 (octahedral, metallic).[40,54,179] This is unwanted from an electronic point of view as the

semiconducting properties of MoS_2 are preferred for electronic use.

Zeng *et al.*'s[179] method further improved the chemical exfoliation process through an electrochemical process. Instead of using *n*-butyl lithium in hexane, they used MoS_2 as the cathode and a lithium foil as an anode, with the whole setup placed in a galvanic cell (see Figure 9e). A measured galvanic discharge controlled the extent of lithiation and provided a better control over the extent of intercalation. This method was conducted at room temperature and required only a few hours instead of days. It yielded about 92% of single-layer MoS_2 sheets. A study conducted by Eda *et al.*[54] addressed the problem of the crystalline structure transformation due to ion intercalation in greater detail. Their study showed that 1T-MoS_2 almost completely (95%) reverted back to 2H-MoS_2 upon annealing at 300 °C.

Solvent-based exfoliation method is relatively new. It was initially proposed by Coleman *et al.* in 2011 and is often referred to as the Coleman method.[182] They began with introducing bulk MoS_2 crystals into organic solvents like *N*-methylpyrrolidone (NMP) and isopropyl alcohol (IPA). The bulk crystals were found to separate into single- and few-layer sheets of MoS_2. The organic solvents were used as they decrease the energy required for layer separation which, followed by sonication, resulted in exfoliation of the suspended flakes into individual 2D crystal layers. This method is sometimes also preferred as use of the organic solvents preserves the 2H-MoS_2 (hexagonal) crystal structure, the semiconducting structure of MoS_2, unlike ion intercalation which tends to render metallic MoS_2 with 1T-MoS_2 (octahedral) crystal structure. The Coleman method was further improved through using an aqueous surfactant followed by high-power sonication, which yielded higher suspension concentration in the solvent.[183] Despite the advantages of this method, there were still a few drawbacks, including the low yield of single-layer sheets and low MoS_2 flake concentration in the solution (0.25 to 0.3 mg/mL).[54,182]

An improvement to the solvent-based exfoliation was proposed by Yao *et al.*,[184] who used a sodium dodecyl sulfate water solution as a surfactant in combination with ball milling of the bulk MoS_2 flakes before introducing them into the solution. Their process had a much higher yield of mono- and bilayer sheets and a higher material concentration of about 0.8−4 mg/mL. A further in-depth study of the effects and duration of sonication on obtained sheet size was conducted by O'Neill *et al.*,[178] resulting in better control of flake size and an even higher reported flake concentration of about 40 mg/mL.

Although chemical exfoliation has much higher yields than mechanical exfoliation, the sonication process does cause scission and tearing of the 2D material sheets, reducing their dimensions down to a few thousand nanometers or even smaller.[40,54,178,179,182,184−186] Small sized MoS_2 flakes are not easily utilized for electronic devices that are directly built on them. However, they can be assembled into MoS_2 thin films or used as colloidal suspensions and even for flexible devices and sensors.[185,186]

A few unconventional methods have been reported which can loosely be categorized as exfoliation methods. Both laser thinning[187] and thermal anneal thinning[188] use heat directly or indirectly to sublimate and thin MoS_2 flakes down to few layers or a single layer. In laser thinning, a laser from a Raman system was systematically scanned over a thick flake of MoS_2 at a higher power.[187] In thermal anneal thinning, MoS_2 flakes on a substrate were annealed at 650 °C in an inert argon environment, causing sublimation of roughly one layer of MoS_2 per hour.[188] Both of these methods caused higher surface roughness due to defect generation, incomplete sublimation of layers, or creation of pinholes in the top layers of the final flakes. Thermal anneal thinning also showed a decrease in flake area along with layer number, indicating sublimation from the flake edges, as well. Layer thinning using argon plasma[189] demonstrated lower surface roughness than the formerly mentioned two methods and could be controlled through the time of exposure to the plasma. This method can also be used with lithographic techniques to pattern MoS_2 heterostructures.

Material Growth. Despite the unique and interesting properties of few-layer MoS_2 flakes, their full potential cannot be realized until the material is possibly obtained on a wafer-scale. Exfoliation techniques have flake size and yield limitations, and they cannot be adopted for large-scale applications like integrated circuit fabrication or other advanced uses. The methods for growing high-quality large-area few-layer MoS_2 crystalline flakes are in high demand toward large-scale implementation of such a unique material.

Until now, thin MoS_2 could be primarily grown from one of three precursors: ammonium thiomolybdate [$(NH_4)_2MoS_4$] solution,[108,143] a thin deposition of elemental molybdenum,[111,117] or molybdenum trioxide [MoO_3] powder.[107,114−116,141,142]

The first precursor, ammonium thiomolybdate, was usually dissolved in dimethylformamide (DMF) and used in solution form.[108,143] This solution was then either coated on a substrate as a thin film or used in vapor form by passing through a bubbler (see Figure 11a). Liu *et al.*[108] dipped their substrate in an ammonium thiomolybdate solution and then pulled the substrate out vertically at a constant low rate in order to obtain a uniform thin film. After the substrate was annealed in a quartz tube with flowing Ar/H_2 at 500 °C and a low pressure of 1 Torr, a second anneal at 1000 °C at a higher pressure of 500 Torr was followed. During the annealing processes, ammonium thiomolybdate was decomposed

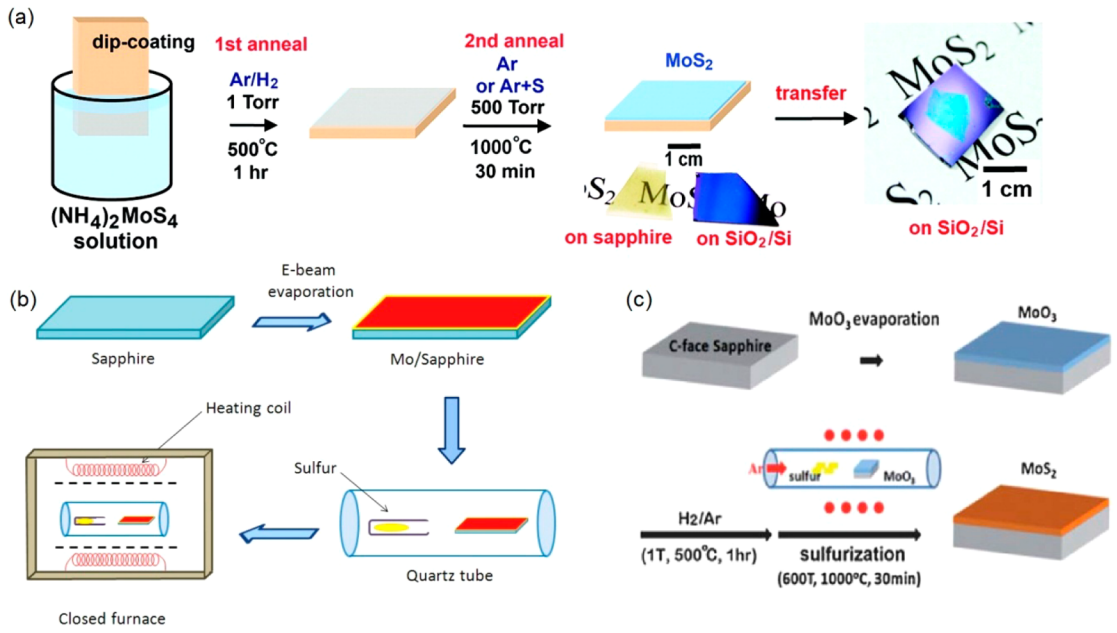

Figure 11. Growth techniques. MoS_2 growth using (a) ammonium thiomolybdate, (b) elemental molybdenum, and (c) molybdenum trioxide as the precursors. Panel a reproduced from ref 108. Copyright 2012 American Chemical Society. Panel b reproduced with permission from ref 111. Copyright 2013 AIP Publishing LLC. Panel c reproduced with permission from ref 116. Copyright 2012 The Royal Society of Chemistry.

into MoS_2, S, H_2S, and NH_3 gases, and MoS_2 was deposited onto the substrate. Sulfur in powder form could also be added to the quartz tube during the second anneal to protect against oxidation of the as-forming film. The final film appeared to be very uniform and consisted of mostly three layers with a few areas having two layers. Although the crystal grain sizes were larger than 160 nm, they were still significantly smaller than those found in exfoliated sheets which are on the order of a few micrometers. Annealing in a sulfur environment yielded a much higher crystallinity of MoS_2 layers. In addition, MoS_2 grown on sapphire substrates showed better quality and larger grains than those grown on SiO_2. FETs fabricated on the grown MoS_2 typically had n-type behavior with an on/off ratio of about $\sim 10^5$ and a field-effect mobility of 6 cm^2/Vs.

Shi *et al.*[143] took a different approach in terms of substrate choice and used single-layer CVD-graphene on Cu foil in order to facilitate van der Waals epitaxy of MoS_2. Graphene was chosen as the growth substrate as its surface is free of dangling bonds and could prove a better growth substrate. MoS_2 was then grown on the substrate using low-pressure CVD at around 400 °C. The precursor was bubbled with argon gas, which was then introduced into the LPCVD chamber to be adsorbed onto the substrate surface. MoS_2 then nucleated at wrinkles on the graphene surface and began to form hexagonal islands of a few hundred nanometers to several micrometers. Increasing the precursor dose was found to result in the islands expanding and coalescing to form complete sheets, with further islands growing on the sheets. It was found that graphene did influence the growth process. In sharp contrast, bare Cu did not show hexagonal MoS_2 island growth. The thickness of the final growth was around 2−5 nm and depended on the precursor dose. Similar work by Liu *et al.*[108] reported a crystal grain size of about 160 nm laterally.

The second method precursor consisted of a very thin layer of molybdenum which was evaporated onto a substrate, followed by sulfurization at a high temperature under inert conditions (see Figure 11b).[111,117] It was found that a higher process temperature resulted in higher quality of grown crystalline MoS_2 layers which seemed to cover the entire substrate[111,117] Zhan *et al.*[117] used lower temperatures of up to 750 °C to grow MoS_2 on the SiO_2 substrate. The grain sizes were found to be 10−30 nm, and the devices fabricated with this grown MoS_2 displayed p-type behavior with field-effect mobilities between 0.004 and 0.04 cm^2/Vs. Laskar *et al.*[111] on the other hand grew MoS_2 on a crystalline sapphire substrate at up to 1000 °C. Their devices based on this MoS_2 showed n-type behavior with significantly higher mobilities of 10−14 cm^2/Vs. In addition, vertically aligned edge-terminated MoS_2 sheets were reported.[190] A ~5 nm thick Mo layer was evaporated on a different substrates. The substrate was kept at the center of a quartz tube furnace having a temperature of 550 °C. Sulfur was placed at an upstream location in the quartz tube, heated to ~220 °C with flowing argon gas at a pressure of 100 mTorr and a flow rate of 100 sccm. Argon flow is continued during the natural cooling of the sample to facilitate vertical growth. The vertically aligned edge-terminated MoS_2 sheets were found to be

unique, and they could be used for catalyst and sensing purposes due to the active edges of the MoS_2 sheets being exposed.

The third choice of precursor, MoO_3 (molybdenum trioxide), has been the most popular for MoS_2 growth.[107,114−116,141,142] All the reports reviewed here have used MoO_3 along with sulfur to grow crystalline MoS_2 layers on a substrate in a quartz tube furnace (see Figure 11c). Balendhran *et al.*[141] were among the first to use this technique. They annealed their substrate in the presence of powdered MoO_3 kept in a crucible and found that the highest quality samples were obtained from the annealing at 830 °C for 180 min, although it was not known if the substrate was uniformly coated with MoS_2 layers. Lee *et al.*[114] next reported using PTAS (perylene-3,4,9,10-tetracarboxylic acid tetrapotassium salt), PTCDA (perylene-3,4,9,10-tetracarboxylic dianhydride), and rGO (reduced graphene oxide) as seed crystals for MoS_2 growth. Aqueous solutions of PTAS, PTCDA, or rGO were spin-coated upon SiO_2 substrates and annealed in N_2 environment at 650 °C. Star-shaped MoS_2 crystals were found to grow around the seed crystals which coalesced to form monolayer to few-layer areas. The rGO-seeded growth was the most uniform with the crystal domain sizes of around 160 nm. FET devices based on the as-prepared MoS_2 flakes were n-type with an on/off ratio of $\sim 10^4$ and a field-effect mobility of 0.02 cm^2/Vs. Lin *et al.*[116] employed a two-step process with the first anneal at 500 °C in a reducing environment of argon and hydrogen, followed by a second anneal at 1000 °C in a sulfur environment. The two-step process was preferred for higher electron mobility of the grown MoS_2. The few-layer MoS_2 film obtained uniformly covered the entire sapphire substrate with a grain size of 160 nm, yielding n-type MoS_2 FET devices with an on/off ratio of $\sim 10^5$ and a field-effect mobility of 0.8 cm^2/Vs. Mann *et al.*[107] used a single anneal process at 600 °C in nitrogen atmosphere but turned off the heating 3 min after the sulfur melted. Although the resultant films did not cover the whole substrate, there were long strips of deposited films that seemed to follow the direction of nitrogen gas flow over the substrate. The films obtained were hundreds of micrometers long with mono- to bilayer areas and had relatively larger grain sizes of 3−5 μm. Fabricated FET devices were n-type with a field-effect mobility of 0.26 cm^2/Vs. Ji *et al.*[142] grew few-layer MoS_2 on a mica substrate which has a very small lattice mismatch with MoS_2 (~2.7%) and could result in epitaxial growth of MoS_2. Compressively strained single-layer films were found to be deposited at 700 °C, which covered most of the substrate.

Apart from these three commonly used precursors, some other precursors have been used, as well. Wu *et al.*[144] used powdered MoS_2, the precursor which was heated at 900 °C and transported using flowing Ar to the substrate at 650 °C. The grown MoS_2 flakes were triangular in shape up to 25 μm in size with high crystallinity. It was found that higher density was easily grown on sapphire substrates as compared to silicon oxide substrates. Yu *et al.*[191] used $MoCl_5$ and elemental sulfur as the precursors, depositing uniform and high-quality monolayer and bilayer MoS_2 on different substrates with grain sizes ranging from tens to hundreds of nanometers at greater than 800 °C. The layer number of the grown MoS_2 flakes can be controlled accurately by control of the amount of $MoCl_5$ used and the growth pressure.

Almost all studies report on the initial growing crystals having a triangular shape. The grains grow to join neighboring MoS_2 crystals at the boundaries and thus form complete films. The grain sizes of grown MoS_2 seem to be much smaller than those obtained using exfoliation techniques. MoS_2 grown on sapphire has consistently higher crystallinity and field-effect mobility than when grown on other substrates such as SiO_2. Najmaei *et al.*[115] recently attempted to provide an explanation of a possible growth model for MoS_2. In this study, MoO_3 nanoribbons along with sulfur were heated to 850 °C in a nitrogen environment. Sulfur concentration and chamber pressure were found to play vital roles in the formation of continuous crystalline MoS_2 films. They suggest two possible growth mechanisms: triangular grains either stop growing once their boundaries meet neighboring grain edges, or a new crystal is nucleated above the current film at the grain boundaries. This boundary-nucleated growth may lead to a completely new independent crystal above the currently formed layer, or it may be an overlapping extension of a grain of the same layer over an adjacent grain.

In this sense, it becomes important to consider the possible defects in CVD-grown MoS_2, their effects on the crystal quality, and electrical properties. Acceptable knowledge of defects could help understand the possible reasons for CVD-grown MoS_2 being inferior to exfoliated MoS_2 and possibly shed some light on where new improvements in growth techniques should be focused. A study by Zhou *et al.*[167] theoretically considered possible defects in CVD-grown MoS_2 depending on the growth conditions. Mo-rich or S-rich growth conditions made the respective defects more energetically favorable; for example, Mo atom replacement by S atoms in the crystal lattice is more favorable in a sulfur-rich condition. Single sulfur vacancies could have the lowest formation energy and most commonly be expected. Single or columnar sulfur vacancies may create unoccupied energy levels about 0.6 eV below the conduction band minimum, which are expected to act as compensation centers in n-type MoS_2. Filling up these vacancies is very likely to improve the material conductivity, being consistent with the higher electrical performance seen in samples annealed in sulfur-rich conditions. Vacancies are also

predicted to increase the material sensitivity of MoS_2-based gas sensors. Electron irradiation could be used to generate such vacancies. The possibility of filling vacancies with atoms of other elements to facilitate doping is also an interesting prospect. The grain boundary defects were also theoretically studied.[167,192] Some common grain boundaries behave like metallic wires and tend to disrupt electrical pathways, negatively affecting field-effect mobilities of CVD MoS_2 flakes.[192,193] MoS_2 edges are rich in unsaturated bonds which can be useful for gas and chemical sensors. MoS_2 grown in Mo-rich growth conditions is predicted to have Mo-terminated states showing a ferromagnetic ground state.[167]

Reviewing the current synthesis methods introduced so far, an urgent need is felt for further improvements in methods to obtain high-quality and large-area crystalline MoS_2. While the most pristine crystalline quality flakes can be obtained through mechanical exfoliation, the yield is extremely low. Ion intercalation techniques suffer from physical and electronic changes to the crystal structure, while solvent-based techniques yield flake sizes too small for fabrication of electronic devices. No exfoliation technique provides much control over the physical size of the obtained flakes. On the other hand, current growth techniques do yield larger flake sizes but often at the cost of crystalline quality and layer number control. In order to fully study and exploit the novel properties of MoS_2, a strong focus is required toward synthesis techniques which can yield highly crystalline wafer-scale MoS_2 growth with good control over layer number, as well.

Doping. Fine-tuning of a material's electronic properties can be achieved through successful doping. As MoS_2 is a quite new material for electronic applications, several theoretical studies[194−197] have provided possible doping strategies and doping species. Two main categories of doping were considered for few-layer MoS_2: substitutional doping and surface adsorption doping. Substitution of either S atoms or Mo atoms by commonly used species creates deep states in the conduction or valence bands and may not play a role of doping of the material in any way. Nb, V, Ta, and Re could be the only species which create shallow energy levels in MoS_2.[194,195,197] Nb, V, and Ta are predicted to be acceptors and Re a donor. S atom substitution could occur when dopant atoms fill up S atom vacancies. However, the doping may not be ineffective due to the generation of deep states.[195,198] In contrast, surface adsorption doping has high potential as it shows lower energy requirement.[195] Alkali metals have predicted strong donor doping characteristics if adsorbed dopants would be used.[195,199] Potassium has already been successfully used as a surface dopant to degenerately dope few-layer MoS_2.[200] Ionic liquids were predicted[195] as well as experimentally confirmed to donate or accept electrons to/from MoS_2 efficiently, as well.[61,119,121]

Electronic Devices. *FET Variants and Circuits.* As compared to graphene which is a semimetal with a zero band gap, MoS_2 is a semiconductor having a much wider indirect (1.29 eV[47,55,141]) as well as direct (∼1.9 eV[47,55,80,141]) band gap in the bulk and monolayer regimes, respectively. The presence of an appreciable band gap makes MoS_2 a viable candidate for next generation electronic devices. The direct large direct band gap in monolayer MoS_2 also opens up a whole new scope in optoelectronic devices.

Simulations and theoretical studies predict MoS_2 devices to have good electron mobilities of ∼200 to ∼400 cm^2/Vs,[95,201,202] very high on/off ratios of $>10^{10}$, and a large transconductance of 4.4 ms/μm.[201] MoS_2 devices showed very high current carrying capabilities of about 5×10^7 A/cm[2203] and small subthreshold swing of about 70 mV/dec.[202] Most MoS_2 FETs have shown n-type behavior. A comparison of silicon devices with MoS_2 devices in line with the ITRS guidelines for low operating power technologies suggests the numerous advantages in favor of MoS_2 devices in terms of higher on/off ratios, much lower power consumption and current leakage, and good switching delay.[202] Due to its 2D structure, MoS_2 is much more resistant to short channel effects as compared to silicon, showing excellent drain-induced barrier lowering (DIBL) of about 10 mV/V,[201] making it theoretically possible to drive down channel length in MoS_2 FETs to sub-10 nm dimensions while having respectable on/off ratios and low current leakage.[174,202] Conductance of MoS_2 devices scale with their channel width and with a shift in the threshold voltage from negative to positive signifying a transition from the depletion mode to enhancement mode by varying the channel width.[204] Significant improvement is still required in contact engineering in order to extract the best performance from practical MoS_2 devices.[174]

The effective mass of carriers in MoS_2 is relatively higher than that of silicon.[202] Higher electron mass allows for thinner channel potential barrier in the off state as well as lower potential barrier in the on state, resulting in increased drive current capabilities and higher on/off ratios. It also allows for greater doping without pushing the Fermi level into the conduction or valence bands. Due to its ultrathin structure and lower density of states, lower gate control is expected.[202] The absence of dangling bonds promotes a very clean surface interface with almost no recombination centers. Also, the ultrathin structure results in the inversion layer charge being closer to the surface as compared to silicon devices.[205] The use of thinner gate oxides should help to gain better gate control. A model developed by Das *et al.*[206] attempted to explain the current flow patterns in layered materials such as MoS_2. The model took each layer in a stacked layered material as a resistor. The van der Waals gap between the layers was also treated as a resistor, and the current tunnels

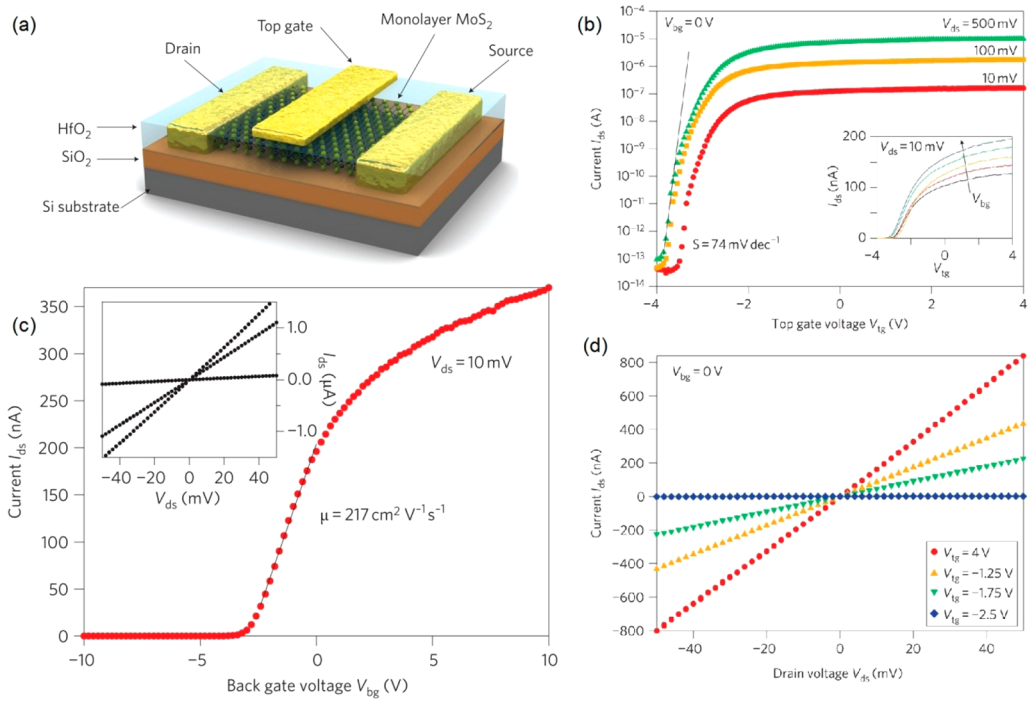

Figure 12. MoS_2 device and performance. (a) Illustration of a top-gate monolayer MoS_2 FET with a high-κ HfO_2 gate dielectric. $I_{ds}-V_g$ device characteristics measured using (b) top gate and (c) back gate. (d) $I_{ds}-V_{ds}$ characteristics plot. Reprinted by permission from Macmillan Publishers Ltd: Nature Nanotechnology, ref 82, copyright 2011.

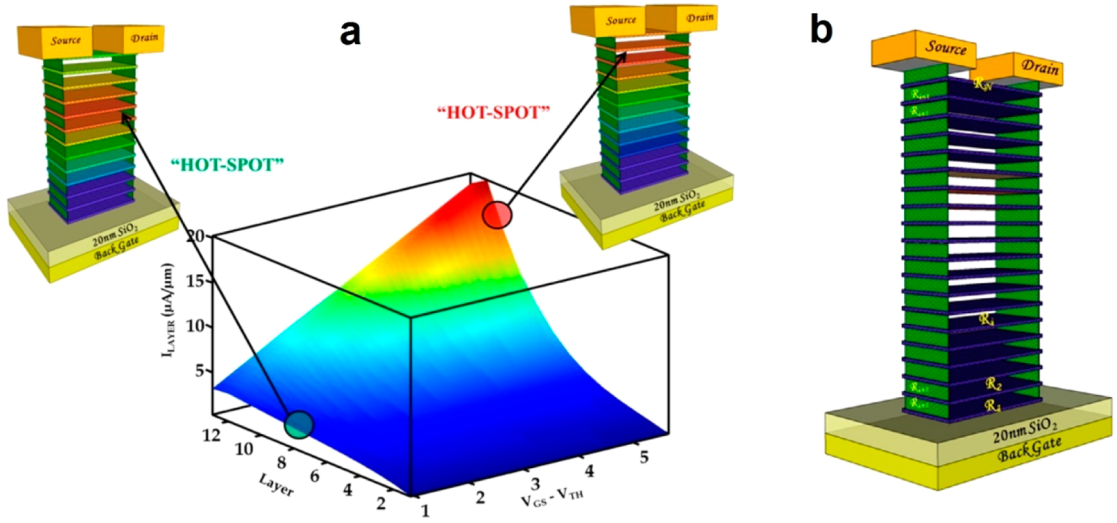

Figure 13. Current flow in MoS_2 layers. (a) Movement of conduction "hot spot" in multilayer MoS_2 devices with variation of gate voltage. (b) Illustration of series-parallel resistor model for multilayer MoS_2 devices. Reproduced from ref 206. Copyright 2013 American Chemical Society.

through layers to travel across layers. The simulation predicted the presence of a "hot spot", that is, a particular layer or set of adjacent layers through which most of the flowing current was concentrated as the gate voltage was varied (see Figure 13) and predicted that the "hot spot" moved toward the upper layers of the stacked structure and farther away from the back gate as the gate voltage was increased.

A major issue with fabricated MoS_2 devices is the extremely low mobility. Thus, improvement of real-life mobility has been the focus of multiple studies.[82,100,109,110,112,113,119,121,201,205,207−211] High-κ gate dielectrics and dielectric engineering in general have been proposed[105] to suppress Coulomb scattering in MoS_2 channels. There have been multiple device studies using various dielectrics. The general prediction was that higher mobilities could be obtainable through high-κ dielectrics.[61,82,110,112,113,119−121,210,211] The very first few-layer MoS_2 FETs with SiO_2 as the gate dielectric layer made by Novoselov *et al.*[2] were of very low mobilities in the range of 0.5−3 cm^2/Vs. A significant improvement in the device performance was

achieved by Radisavljevic *et al.*[82] with the use of a HfO_2 high-κ gate dielectric (see Figure 12). The top-gated MoS_2 FETs demonstrated a large jump in the mobility up to about 200 cm^2/Vs along with an on/off ratio of 10^8. This achievement was attributed to suppression of Coulomb scattering and modification of phonon dispersion. Al_2O_3 as a high-κ dielectric has been applied to MoS_2 FETs, leading to high mobilities of ~100 cm^2/Vs for the bottom-gated structure,[209] ~170 cm^2/Vs for the top-gated structure,[113] and 517 cm^2/Vs for the dual-gated structure.[211] The use of ionic liquids as a dielectric material resulted in ambipolar characteristics and suggests an improvement in the mobility attributed to the dielectric properties as well as a reduction in the Schottky barrier at the metal/MoS_2 contacts.[119,121] Polymer-gated MoS_2 FETs have been also presented.[112,120] Poly(ethylene oxide) used with lithium perchlorate ($LiClO_4$)[112] was found to promote a three-order improvement in the mobility from ~0.1 to ~150 cm^2/Vs, attributed partially due to the dielectric effect of the polymer and partially through reduction of contact resistance. Polymethyl methacrylate (PMMA)[120] was used as the gate dielectric as well as the substrate of MoS_2 FETs, resulting in ambipolar device characteristics and a large mobility of 470 cm^2/Vs. This large enhancement in the mobility was explained to be due to the smooth PMMA substrate with no chemical bonding.[120]

This is quite interesting as it brings up two possible causes of lower mobility in MoS_2: substrate effects and contact effects. The importance of selection of the substrate has already been seen in the crystal as well as electrical quality of few-layer MoS_2 obtained *via* growth processes. Substrate interactions with MoS_2 flakes have also been important issues in the study of the 2D MoS_2. Factors like surface roughness and sheet ripples strongly affect mobility, while dangling bonds have been shown to introduce deep energy states to the energy structure of MoS_2. The field-effect mobility of devices was recently found to be an order of magnitude greater when placed on hexagonal boron nitride substrates, having inert surfaces relatively free of dangling bonds, as compared to mobilities measured when on silicon oxide substrates which have a high density of dangling bonds on the surface.[212] MoS_2 was found to be sensitive even to atmospheric humidity, which could adsorb on the material surface and resulted in a hysteresis in the transfer characteristics.[175]

Studying the contact effects on MoS_2 and engineering contact barriers is another push to practically realize the theoretically predicted field-effect mobilities of MoS_2. An *ab initio* study by Popov *et al.*[208] compared gold and titanium contacts to MoS_2. It was suggested that gold, a common metal for electrodes in many electronic devices, is not an ideal contact metal material for MoS_2 for multiple reasons. Due to the material geometries of MoS_2 flakes, gold and titanium, there is physically less space between Ti atoms and the S atoms of MoS_2, resulting in stronger contact adhesion of Ti to MoS_2. There is thus also a greater overlap of titanium's atomic orbitals with MoS_2 as compared to that with gold. For efficient charge transfer from contacts to MoS_2, the electronic states at the Fermi level of the contact metal must strongly overlap and align with that of MoS_2. The Fermi level of gold turns out to be less aligned with MoS_2 as compared to titanium, resulting in poor electrical contact properties. In addition, metal−MoS_2 contacts cannot be completely ohmic as a Schottky barrier always exists. As the barrier width was greater for gold as compared to titanium owing to greater work function differences along with the above reasons, there is a reduced amount of charge transfer to MoS_2. Titanium was thus predicted to be a better contact material to MoS_2 as compared to gold[208] and is more commonly used. Scandium has a lower work function which could match the density of states in MoS_2 much better than Au and other metals. Scandium/MoS_2 contacts were found to be of small contact resistance, and the reported mobility of 700 cm^2/Vs[110] was the highest reported so far. Potassium-doped contacts for MoS_2 devices demonstrated ohmic behavior,[200] also suggesting that a low work function metal is better than a high work function metal as the electrodes in MoS_2 devices.

Many application-oriented devices based on MoS_2 have been developed. Taking advantage of the flexible and transparent nature of few-layer MoS_2, Chang *et al.* reported[210] on MoS_2 FETs with high-κ dielectrics fabricated on flexible substrates, which had a typical on/off ratio of 10^7, subthreshold slope of ~82 mV/dec, and a low field mobility of 30 cm^2/Vs and could be bent to a radius of 1 mm with stable performance (see Figure 14b).

Integrated circuits based on monolayer[214] and bilayer[215] MoS_2 were successfully demonstrated, although they were only in the proof-of-concept stage. Hybrid devices using MoS_2 along with other materials have been studied as well as reported. A density functional theory (DFT) study of stacked monolayer graphene−MoS_2 heterostructures[216] predicted the introduction of a small band gap in graphene due to MoS_2 and significantly higher mobilities in MoS_2 due to graphene. This would make a very interesting practical device. An inverter with p-type carbon nanotube and an n-type MoS_2 FETs was fabricated with a reported gain of 1.3.[217] A nonvolatile memory cell with monolayer MoS_2 as the channel semiconductor and single-layer graphene as the floating gate (see Figure 14a) showed very stable operation and was estimated to be able to retain 30% of the initial stored charge even after 10 years by observing the shift in threshold voltage over 10^4 s and extrapolating the observed rate of threshold voltage shift until it reached zero.[213]

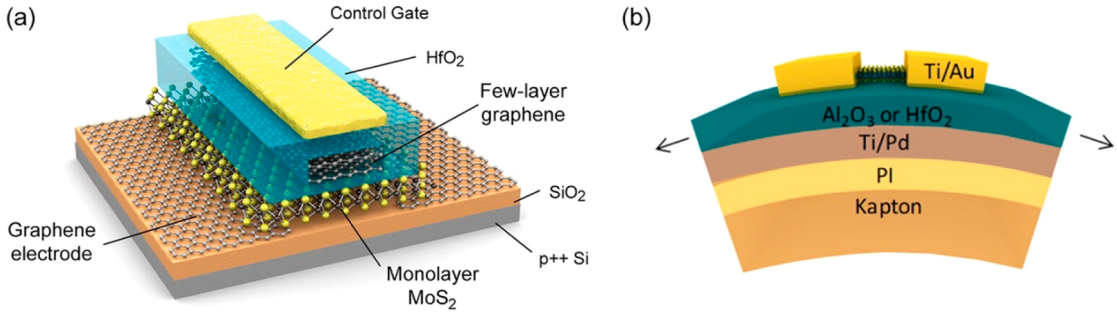

Figure 14. Other device variants and applications. (a) Illustration of MoS_2/graphene flash memory cell. (b) Illustration of a flexible MoS_2 device fabricated on a flexible substrate. Panel a reproduced from (a) ref 213. Copyright © 2013 American Chemical Society. Panel b reproduced from ref 210. Copyright 2013 American Chemical Society.

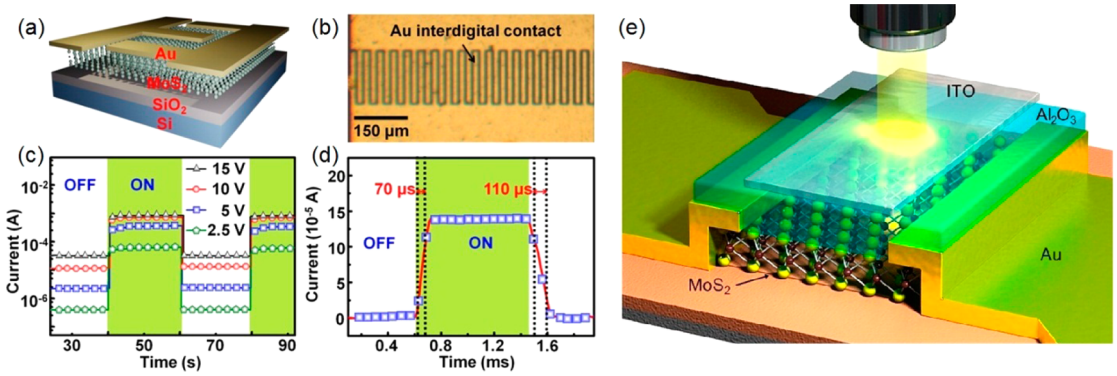

Figure 15. Optoelectronic devices. (a) Illustration and (b) optical image of a high-performance rugged metal−semiconductor−metal photodetector (MSM-PD) along with its on/off ratio characteristics (c,d). (e) Illustration of a monolayer optoelectronic device with a high-κ Al_2O_3 gate dielectric and an ITO top gate. Panels a-d reproduced from ref 134. Copyright © 2013 American Chemical Society. Panel e reproduced from ref 218. Copyright 2012 American Chemical Society.

Optoelectronic Devices. The direct transition optical gap in few-layer MoS_2 opens the doors to interesting optoelectronic applications. The very first MoS_2 optoelectronic device was reported by Yin *et al.*[177] The device was a phototransistor fabricated on monolayer MoS_2 and showed an appreciable photocurrent with incident light of wavelengths less than 670 nm or photon energy greater than the direct transition gap of MoS_2 (1.83 eV). The device had short switching times of ∼50 ms and high photosensitivity of ∼1 mA/W. Devices fabricated by Lee *et al.*[218] on mono-, bi-, and trilayer MoS_2 flakes with an ITO top gate and high-κ Al_2O_3 gate dielectric (see Figure 15e) sensitively responded to green (550 nm) and UV (365 nm) light for mono-, bi-, and trilayer flakes while only the bi- and trilayer flakes responded well to red light (680 nm). Their thickness-modulated optical band gaps were found to be ∼1.82, ∼1.65, and ∼1.35 eV for mono-, bi-, and trilayer flakes, respectively, confirming thickness and confinement modulated band gaps in MoS_2. However, they showed long response time of 1.5, 1, and ∼0.3 s and an exponential decay when the light source was switched off. Choi *et al.*[219] fabricated multilayer (10−60 nm) MoS_2 back-gate phototransistors on silicon substrate with a high-κ Al_2O_3 gate dielectric. Their devices responded to a much wider range of photon wavelengths of <900 nm with an appreciably larger photoresponsivity of >100 mA/W and a short carrier lifetime of 1.27 ns. They found that ∼30 nm thick MoS_2 flakes absorbed only 60% of the incident light (630 nm). Zhang *et al.*[73] performed an extensive study on the effect of atmospheric adsorbates on CVD-grown MoS_2 through the photoresponse. Comparisons between the device performance in ambient air conditions and in vacuum confirmed, upon atmospheric adsorption, an increase in threshold voltage, 1 order decrease in electron field-effect mobility, almost 3-fold decrease in photoresponsivity, a more than 2.5-fold drop in photogain, and a huge drop in photocurrent relaxation time constant from 500 to 3 s. Air adsorbates were suggested to act as p-dopants which decrease the n-type behavior of MoS_2 FET devices. Notably, this behavior was reversible as placing the devices back in vacuum restored the performance of the devices. These observations further indicated that MoS_2-based devices are highly sensitive to the surface and interface conditions. In metal−semiconductor−metal photodetectors (MSM-PDs) (see Figure 15a,b), where the semiconductor was chemically grown trilayer MoS_2,[134] large improvements in photoresponsivity of 0.57 A/W, fast response time of ∼70 μs, short recovery time of ∼110 μs, and a photogain up to 13.3 over the visible

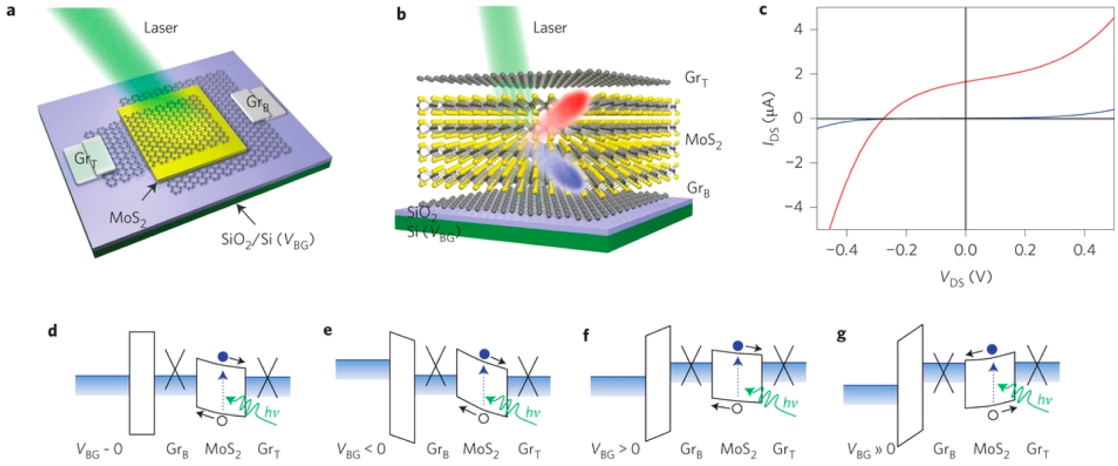

Figure 16. GMG heterostructure and band diagrams. (a,b) Illustrations of the graphene/MoS_2/graphene (GMG) structure. (c) Current−voltage characteristics of a GMG device in the dark (blue) and when illuminated (red). (d−g) Evolution of the device's band alignment and photogenerated electrons and holes (in the case of laser illumination) for $V_{BG} = 0$ (d), $V_{BG} < 0$ (e), $V_{BG} > 0$ (f), and $V_{BG} \gg 0$ (g). Reprinted by permission from Macmillan Publishers Ltd: Nature Nanotechnology, ref 222, copyright 2013.

spectrum range were achieved. Importantly, the devices were workable at higher temperatures of 200 °C with a unity gain at 250 °C, proving to be capable of handling harsh environments. The improvement to device photogain was attributed to surface-defect-trapped photocarrier injection from the metal contacts to MoS_2, which cause a decrease in the contact−MoS_2 Schottky barrier height. A recent report[220] has pushed the photoresponsivity up to 880 A/W for monolayer MoS_2 devices, a factor of 10^5 higher than that of graphene detectors reported so far. The improvement was attributed to better mobility figures and improved quality of the metal−MoS_2 contact. A heterostructure of graphene stacked on MoS_2[221] has further elevated the photoresponsivities up to 10^7 A/W due to trapping of generated photocarriers in graphene.

Heterostructure Devices. While purely MoS_2 devices have been gaining attraction, there have also been advances in designing heterostructures which use other materials like graphene in conjunction with MoS_2 in pursuit of novel devices utilizing the unique properties of more than just one material.[223] One of the first heterostructures was by Britnell *et al.*[224] using a vertically stacked graphene/MoS_2/graphene (GMG) sandwich structure (see Figure 16a,b) as a tunneling transistor with MoS_2 acting as an ultrathin tunneling barrier between two graphene electrode layers. While a majority of the paper focused on using hexagonal boron nitride (hBN) as the insulator, the authors mentioned using MoS_2, as well, yielding an improvement in the on/off ratio from ∼50 when using graphene/hBN to $\sim 10^4$ when using graphene/MoS_2. As their observations and results pertain to structures using MoS_2, as well, the principles of the heterostructure shall also be reviewed here. The vertical GMG as a tunneling transistor was further studied by Myoung *et al.*[225]

In field-effect transistors, the source/drain and channel region are comparatively thick, on the order of a few tens of nanometers. The source, drain, and channel regions of the GMG structures on the other hand had few- to sub-nanometer dimensions.[224,225] Monolayers of graphene were used as source/drain contacts. This brought about another important distinction: while FETs have metal contacts with a large concentration of free carriers and thus play only a passive role in the device functioning, the GMG devices used the change in density of states (DOS) of graphene electrodes to control device operation.[224−226] Upon application of a positive back-gate voltage V_{BG}, the Fermi level E_F of both the bottom graphene electrode (Gr_B) as well as top graphene electrode (Gr_T) increased due to low electric field screening through Gr_B and MoS_2 (see Figure 16d−g). While Gr_B allowed most of the electric field to penetrate through it, its low screening factor resulted in the increase in E_F of Gr_B always being greater than that of Gr_T. The increase in E_F also resulted in a decrease in tunneling barrier height Δ and thus an increase in tunneling current I. As graphene's cone-like band structure is symmetrical about its Dirac point, the tunneling current increased when E_F moved away from the Dirac point and more DOS were available for electron conduction. The symmetry of the device response was determined by the alignment of the graphene electrodes with the insulator. In the case of MoS_2, graphene's Fermi level E_F is closer to monolayer MoS_2's conduction band (∼0.5 eV). The device response was thus asymmetrical, having a higher electron tunneling current as compared to hole tunneling current due to a smaller tunneling barrier experienced by electrons. Owing to the device's ultrathin structure and resultant short channel, highly sensitive gate control was observed. Tunneling current thus did not saturate and increased with increasing V_b.

The low DOS of graphene was crucial to the functioning of the GMG structure and was further exploited by Myoung *et al.*[225] by using an armchair graphene

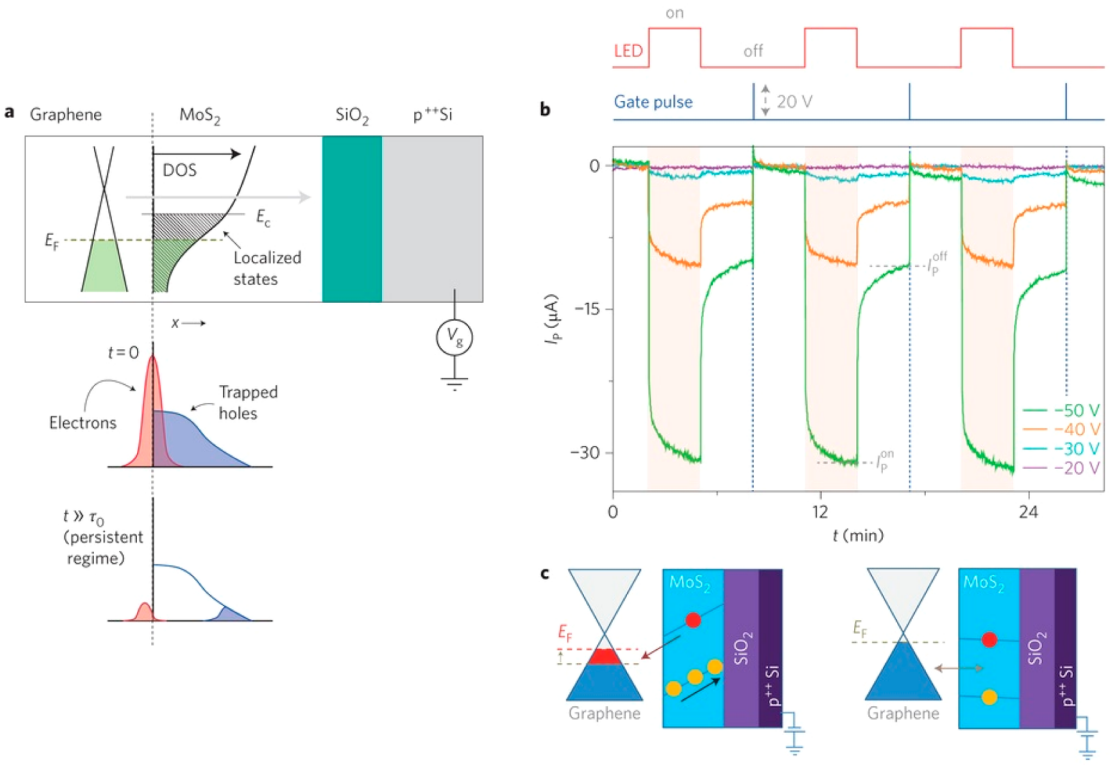

Figure 17. Photoresponsive memory heterostructure. (a) Illustration showing the change in carrier distribution with time. Illumination pulse is given at time $t = 0$. (b) Photoresponse graph with gate pulses and applied negative back-gate voltages. (c) Illustration of carrier flow and Fermi level positions of graphene and MoS_2 with negative (left) and positive (right) gate voltages applied. Reprinted by permission from Macmillan Publishers Ltd: Nature Nanotechnology, ref 227, copyright 2013.

nanoribbon (AGNR) as Gr_T. The DOS of graphene nanoribbons had a one-dimensional dependence which manifested in the form of repetitive current peaks in the $I-V_b$ curves corresponding with changes in the AGNR's DOS at E_F as V_b was varied. GMG heterostructures used as spin-polarized devices were also simulated. It was also predicted that holes would experience strong spin-polarization due to greater spin-splitting in MoS_2's valence band as compared to that in the conductance band.

The direct band gap of MoS_2 was also exploited to fabricate optical devices. Yu *et al.*[222] used the GMG structure to obtain gate-dependent photocurrent. The MoS_2−graphene contact interfaces formed Schottky barriers whose depletion regions within MoS_2 merged to form smooth band bending due to the few-layer MoS_2 flakes being thinner than the Schottky barrier depletion width, creating a built-in potential within the structure. Substrate-induced p-doping of Gr_B was expected to result in a greater MoS_2-Gr_B Schottky barrier height as compared to that of MoS_2-Gr_T, causing the MoS_2 bands to bend downward toward Gr_T (see Figure 16d−g). This naturally built-in potential slope within the structure resulted in separation of photogenerated electrons and holes within MoS_2 toward Gr_T and Gr_B, respectively. A negative back-gate voltage V_{BG} increased MoS_2 band's downward bending toward Gr_T, while a positive V_{BG} caused the opposite, allowing variable control of the degree of photogenerated carrier separation and thus photogenerated current. A top-gated device allowed for greater electric field within the structure and thus greater band bending for $V_{BG} \gg 0$ causing photocurrent inversion due to reversed separation of the photogenerated carriers. In contrast to graphene-only devices in which photocurrent was generated at the contact interfaces, the GMG devices showed photocurrent generation throughout the graphene−MoS_2 overlapping area.

Roy *et al.*'s MoS_2-based heterostructures[227] have shown promise as a photoresponsive memory device displaying persistent photoconductivity (PPC). Unlike the previous GMG heterostructures, metallic contacts were used and only a single layer of graphene was part of the structure. The devices were fabricated by transferring graphene onto few-layer MoS_2 flakes exfoliated on a Si/SiO_2 substrate followed by deposition of metallic source/drain contacts. The device operation took advantage of the built-in potential developed at the interface between graphene and MoS_2 (see Figure 17a). Illumination of the device with simultaneous application of a negative back-gate voltage resulted in an increase from the preillumination state negative photocurrent ($I_P = 0$) to I_P^{ON} (see Figure 17b). The negative back-gate voltage was explained to have forced photogenerated electrons within MoS_2 to move to the graphene layer while the photogenerated holes remained within MoS_2

(see Figure 17c). As the graphene layer was found to be p-doped, the injection of electrons resulted in upward shift of the Fermi level toward to the Fermi−Dirac point, increasing the device resistance and hence a negative photocurrent. Upon removal of the illumination source, the negative photocurrent would not revert back to the preillumination value I_P. Instead, it would settle at a finite value I_P^{OFF}. This phenomenon was understood to be due to the inability of the separated photogenerated carriers in graphene and MoS_2 to recombine given the presence of the graphene−MoS_2 interface's built-in potential. Application of a high positive back gate was observed to restore the photocurrent back to $I_P = 0$ as it would allow the trapped carriers to overcome the built-in potential and recombine. Such persistent photoconductivity was quite interesting and opened up new possibilities and applications for such heterostructures.

Sensors. The 2D structure of MoS_2 flakes provides not only new electronic and optoelectronic avenues but also high surface-to-area ratios. These unique merits make few-layer MoS_2 flakes excellent sensing elements to many adsorbates. A first-principle study[228] examined the adsorption and diffusion of gaseous hydrogen on the MoS_2 surface and revealed monolayer MoS_2 to have a high sensing ability and a preferential bonding of hydrogen to sulfur atoms or in sulfur vacancies on the MoS_2 surface. An applied strain could lower the energy barrier to adsorption on the MoS_2 surface. Another study[229] used first-principle calculations to determine adsorption energies of various gaseous species on MoS_2, preferred adsorption sites, as well as surface charge distributions upon adsorption. Charge transfer between adsorbed gaseous species and MoS_2 was predicted to be small and partial with gases such as H_2, O_2, H_2O, NO, NO_2, and CO acting as charge acceptors while NH_3 was expected to behave as a charge donor. The low predicted adsorption energies coupled with large predicted adsorption distances pointed to physisorption of gaseous molecules on the MoS_2 surface rather than chemisorption processes, suggesting quick and reversible sensor response. This was observed in a practical study backed by theoretical calculations which reported the effect of adsorbed gases on the photoluminescence intensity from studied flakes.[147] Exposure to gaseous species such as O_2 and H_2O caused an increase in PL intensity by almost 2 orders and was found to be directly dependent on the gas pressure. Changes in gas pressure were almost immediately reflected in the form of changes in observed PL intensity, lending credence to the adsorption mechanism being of a physisorption nature. Two studies used MoS_2 in aqueous suspensions to sense NO_2 with sensitivities as high as 20[230] and 2 ppb[231] (using reduced graphene oxide and Pt nanoparticles). MoS_2 FET sensors in NO environment[232] displayed a very high sensitivity (0.3 to 2 ppm). Monolayer MoS_2 FET NO sensor performance was found to be unstable despite being faster, while bi- to quadlayer sensors had stable performance. Another report[233] on NO_2, NH_3, and humidity MoS_2 FET sensors presented a sensitivity of the five-layer MoS_2 flake higher than that of the two-layer samples, with unstable performance of monolayer samples. Sensitivity to gases was found to be tunable through gate voltage (for the FET structure), enhancing sensitivity for NO_2 and decreasing sensitivity for NH_3 with application of positive back-gate voltage. This was explained by electron donor and acceptor natures of NH_3 and NO_2, respectively. It was found that electron donor gases caused higher sensitivity than electron acceptor gases. Exposure to light was also observed to increase device sensitivity and decrease recovery time, depending on the gas being sensed. MoS_2 has also shown sensitivity toward triethylamine,[234] a decomposition product of a nerve gas agent. Triethylamine is a strong electron donor, and exposure of MoS_2 to triethylamine increases its conductivity with increasing gas concentration. The authors of this work postulated the importance of the exposed p-orbitals of the S atoms as the reason for this high sensitivity due to their positively charged nature.

Other MoS_2 Morphologies. While huge research interests are focused on 2D MoS_2 sheets, other nanostructures like MoS_2 nanotubes and nanoribbons have received attention for their confinement-induced physics and properties. As MoS_2-based nanotube and nanoribbon research is still in its infancy, much of the reported work is theoretical and addresses the physics borne from these morphologies such as the band structure, electrical properties, and magnetic behavior.

Nanoribbons. MoS_2 nanoribbons are basically very thin nanosized strips having widths much smaller than their lengths. Their narrow widths cause quantum confinement which gives rise to dimension-related variation and tailoring of material properties and behavior. There are two types of MoS_2 nanoribbons based on the lengthwise terminating edges: armchair and zigzag. Armchair nanoribbon length edges terminate in either Mo or S atoms, as seen in Figure 18b, while zigzag nanoribbons terminate in repeated pairs of Mo/S atoms as seen in Figure 18a. Zigzag MoS_2 nanoribbons are predicted to display metallic behavior, while armchair nanoribbons are predicted to be semiconducting.[166,235] Zigzag nanoribbons are of magnetic behavior, with the magnetic moment concentrated at the edges of the nanoribbon.[166,236] The magnetic edge moment is attributed to sulfur vacancies on the edges.[237] Creation of a S vacancy in a S edge with 50% coverage of S atoms increases the magnetic moment, while creation of a similar S vacancy in a S edge with 100% coverage of S atoms decreases the magnetic moment. Triple sulfur vacancies inside the material[235] as well as adsorption of adatoms like Co at the edges[235] also create magnetic moments. Application of strain to zigzag MoS_2 nanoribbons could cause a four-stage evolution of electronic phase transitions (magnetic metal ↔ half-metal

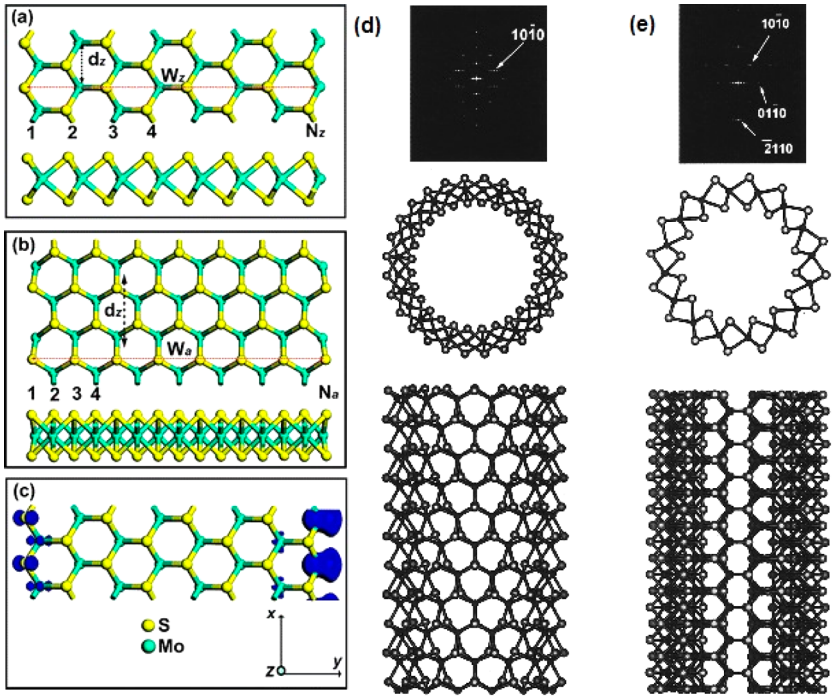

Figure 18. Nanoribbons and nanotubes. Illustrations of (a) zigzag and (b) armchair MoS_2 nanoribbons. (c) Spatial spin distribution of magnetic moments at the edges of a zigzag MoS_2 nanoribbon. Simulated diffraction patterns (top), view from the tube axis (middle), and *c*-axis (bottom) of (d) zigzag and (e) armchair MoS_2 nanotubes. Panels a–c reproduced from ref 166. Copyright 2008 American Chemical Society. Panels d and e reproduced from ref 240. Copyright 2000 American Chemical Society.

semiconductor ↔ half-metal ↔ magnetic metal) with greater stability, showing a wide range of tunability of electronic and magnetic properties.[236] The band gap of armchair nanoribbons depends on the nanoribbon width. Application of transverse magnetic fields could decrease the band gap until the band gap becomes zero beyond a critical value of electric field,[238,239] while perpendicular electric fields have no effect on monolayer armchair MoS_2 nanoribbons. The application of transverse electric fields also causes armchair nanoribbons to switch between diamagnetic and magnetic states.[239]

Nanotubes. There have been a few reports of MoS_2 nanotube (MNT) growth, such as heating MoS_2 powder covered by Mo foil at 1300 °C,[240] through catalyzed self-assembly,[241] sulfurization of $Mo_6S_2I_8$ nanowires,[242] and transformation of MoO_3 nanobelts into MoS_2 nanotubes.[243] Armchair MNTs (see Figure 18e) exhibit a small indirect band gap and a moderate direct band gap while zigzag MNTs (see Figure 18d) exhibit a small direct band gap[244] which can have potential optical applications. Their band gaps are affected by confinement and can be tailored through tube diameter variation. MNTs could have fewer defects than CNTs.[245] However, defects in MNTs may cause metallic behavior.[246] MNTs can be stretched up to 16% without breaking and have higher strain energies than CNTs but have lower tensile stress than CNTs.[245] MNTs also inherit the low friction properties of their layered counterparts.[247] MNTs showed A and B excitons in the UV–vis spectra like 2D MoS_2 sheets, albeit with a slight red shift as compared to those seen in few-layer MoS_2 sheets due to confinement effects.[242] Lithium-doped MNTs were found to have high magnetic susceptibility and remain paramagnetic even at extremely low temperatures.[248]

CONCLUSION

Like graphene triggering a wave of research interest in ultrathin 2D materials, now few-layer MoS_2 has created another wave in ultrathin devices and physics. In order for few-layer MoS_2 to be applicable, the techniques to obtain wafer-scale high-quality crystalline MoS_2 sheets are urgently required. The atomically thin MoS_2 flakes make them highly sensitive to environmental and substrate effects, which have been theoretically and experimentally confirmed to affect almost every aspect of the material's properties from the material growth mechanisms, carrier transport processes, the performances of a variety of few-layer MoS_2-based devices, *etc*. The interactions between few-layer MoS_2 flakes and their surface adsorbates dominate the physical properties of the 2D material and still need in-depth study and understanding. The factors affecting electron field mobility and device performance are not yet fully understood and require further theoretical as well as experimental study. The direct optical band gap of few-layer MoS_2 coupled with spin and valley polarization physics holds the potential for a vast new range of optical and optoelectronic

applications. The high flexibility, low power consumption, and excellent electronic properties promote the material to be of substantial potential in future flexible and transparent electronic circuits. In addition, there is much more to be gained from heterostructures of MoS_2 along with other materials, a large family of novel materials which possess rich functionalities in comparison with pure few-layer MoS_2 flakes.

Conflict of Interest: The authors declare no competing financial interest.

REFERENCES AND NOTES

1. Schwierz, F. Nanoelectronics: Flat Transistors Get Off the Ground. *Nat. Nanotechnol.* **2011**, *6*, 135–136.
2. Novoselov, K. S.; Jiang, D.; Schedin, F.; Booth, T. J.; Khotkevich, V. V.; Morozov, S. V.; Geim, A. K. Two-Dimensional Atomic Crystals. *Proc. Natl. Acad. Sci. U.S.A.* **2005**, *102*, 10451–10453.
3. Yoffe, A. Electronic Properties of Low Dimensional Solids: The Physics and Chemistry of Layer Type Transition Metal Dichalcogenides and Their Intercalate Complexes. *Solid State Ionics* **1990**, *39*, 1–7.
4. Yoffe, A. D. Electronic Properties of Two Dimensional Solids: The Layer Type Transition Metal Dichalcogenides. *Festkörperprobleme 13*; Springer: Berlin, 1973; Vol. 13, pp 1−29.
5. Doran, N. J. Electronic Structure and Band Theory of Transition Metal Dichalcogenides. *Physica B+C* **1980**, *99*, 227–237.
6. Castro Neto, A. H. Charge Density Wave, Superconductivity, and Anomalous Metallic Behavior in 2D Transition Metal Dichalcogenides. *Phys. Rev. Lett.* **2001**, *86*, 4382–4385.
7. Lieth, R. M. A.; Terhell, J. C. J. M. *Transition Metal Dichalcogenides*; Springer: Berlin, 1977; pp 141−223.
8. Umrigar, C.; Ellis, D.; Wang, D.-S.; Krakauer, H.; Posternak, M. Band Structure, Intercalation, and Interlayer Interactions of Transition-Metal Dichalcogenides: TiS_2 and Li-TiS_2. *Phys. Rev. B* **1982**, *26*, 4935–4950.
9. Withers, R. L.; Wilson, J. A. An Examination of the Formation and Characteristics of Charge-Density Waves in Inorganic Materials with Special Reference to the Two- and One-Dimensional Transition-Metal Chalcogenides. *J. Phys. C: Solid State Phys.* **1986**, *19*, 4809–4845.
10. Rossnagel, K. On the Origin of Charge-Density Waves in Select Layered Transition-Metal Dichalcogenides. *J. Phys.: Condens. Matter* **2011**, *23*, 213001.
11. Christy, R. I. Sputtered MoS_2 Lubricant Coating Improvements. *Thin Solid Films* **1980**, *73*, 299–307.
12. Fleischauer, P. D.; Bauer, R. Chemical and Structural Effects on the Lubrication Properties of Sputtered MoS_2 Films. *Tribol. Trans.* **1988**, *31*, 239–250.
13. Wahl, K. J.; Singer, I. L. Quantification of a Lubricant Transfer Process That Enhances the Sliding Life of a MoS_2 Coating. *Tribol. Lett.* **1995**, *1*, 59–66.
14. Wu, C.; Hou, S. X.; Zhang, H. Q.; Jia, X. M. Study and Evaluation on Dispersion of Molybdenum Disulfide in Aqueous Solution. *Adv. Mater. Res.* **2013**, *750−752*, 2175–2178.
15. Ripoll, M. R.; Simič, R.; Brenner, J.; Podgornik, B. Friction and Lifetime of Laser Surface-Textured and MoS_2-Coated Ti_6Al_4V under Dry Reciprocating Sliding. *Tribol. Lett.* **2013**, *51*, 261–271.
16. Feng, X.; Tang, Q.; Zhou, J.; Fang, J.; Ding, P.; Sun, L.; Shi, L. Novel Mixed-Solvothermal Synthesis of MoS_2 Nanosheets with Controllable Morphologies. *Cryst. Res. Technol.* **2013**, *48*, 363–368.
17. Park, T. Y.; Nam, I.-S.; Kim, Y. G. Kinetic Analysis of Mixed Alcohol Synthesis from Syngas over K/MoS_2 Catalyst. *Ind. Eng. Chem. Res.* **1997**, *36*, 5246–5257.
18. Del Valle, M.; Cruz-Reyes, J.; Avalos-Borja, M.; Fuentes, S. Hydrodesulfurization Activity of MoS_2 Catalysts Modified by Chemical Exfoliation. *Catal. Lett.* **1998**, *54*, 59–63.
19. Faye, P.; Payen, E.; Bougeard, D. Cluster Approach of Active Sites in an MoS_2 Catalyst. *J. Mol. Model.* **1999**, *5*, 63–71.
20. Tye, C. T.; Smith, K. J. Catalytic Activity of Exfoliated MoS_2 in Hydrodesulfurization, Hydrodenitrogenation and Hydrogenation Reactions. *Top. Catal.* **2006**, *37*, 129–135.
21. Wu, Z.; Fang, B.; Wang, Z.; Wang, C.; Liu, Z.; Liu, F.; Wang, W.; Alfantazi, A.; Wang, D.; Wilkinson, D. P. MoS_2 Nanosheets: A Designed Structure with High Active Site Density for the Hydrogen Evolution Reaction. *ACS Catal.* **2013**, *3*, 2101–2107.
22. Yun, J.-M.; Noh, Y.-J.; Yeo, J.-S.; Go, Y.-J.; Na, S.-I.; Jeong, H.-G.; Kim, J.; Lee, S.; Kim, S.-S.; Koo, H. Y.; *et al.* Efficient Work-Function Engineering of Solution-Processed MoS_2 Thin-Films for Novel Hole and Electron Transport Layers Leading to High-Performance Polymer Solar Cells. *J. Mater. Chem. C* **2013**, *1*, 3777.
23. Fontana, M.; Deppe, T.; Boyd, A. K.; Rinzan, M.; Liu, A. Y.; Paranjape, M.; Barbara, P. Electron−Hole Transport and Photovoltaic Effect in Gated MoS_2 Schottky Junctions. *Sci. Rep.* **2013**, *3*, 1634.
24. Bernardi, M.; Palummo, M.; Grossman, J. C. Extraordinary Sunlight Absorption and One Nanometer Thick Photovoltaics Using Two-Dimensional Monolayer Materials. *Nano Lett.* **2013**, *13*, 3664–3670.
25. Shanmugam, M.; Durcan, C. A.; Yu, B. Layered Semiconductor Molybdenum Disulfide Nanomembrane Based Schottky-Barrier Solar Cells. *Nanoscale* **2012**, *4*, 7399–7405.
26. Jamieson, I.; Jakovidis, G. Thin Film Texture of Layered Molybdenum Disulphide for Photovoltaic Cells. *IEEE Xplore* **2004**, 117–120.
27. Kwon, J.-H.; Ahn, H.-J.; Jeon, M.-S.; Kim, K.-W.; Ahn, I.-S.; Ahn, J.-H.; Wang, G.; Ryu, H.-S. The Electrochemical Properties of Li/TEGDME/MoS_2 Cells Using Multi-wall Carbon Nanotubes as a Conducting Agent. *Res. Chem. Intermed.* **2010**, *36*, 749–759.
28. Zhang, C.; Wu, H. B.; Guo, Z.; Lou, X. W. Facile Synthesis of Carbon-Coated MoS_2 Nanorods with Enhanced Lithium Storage Properties. *Electrochem. Commun.* **2012**, *20*, 7–10.
29. Liu, H.; Su, D.; Zhou, R.; Sun, B.; Wang, G.; Qiao, S. Z. Highly Ordered Mesoporous MoS_2 with Expanded Spacing of the (002) Crystal Plane for Ultrafast Lithium Ion Storage. *Adv. Energy Mater.* **2012**, *2*, 970–975.
30. Chang, K.; Chen, W. *In Situ* Synthesis of MoS_2/Graphene Nanosheet Composites with Extraordinarily High Electrochemical Performance for Lithium Ion Batteries. *Chem. Commun.* **2011**, *47*, 4252–4254.
31. Fang, X.; Guo, X.; Mao, Y.; Hua, C.; Shen, L.; Hu, Y.; Wang, Z.; Wu, F.; Chen, L. Mechanism of Lithium Storage in MoS_2 and the Feasibility of Using Li_2S/Mo Nanocomposites as Cathode Materials for Lithium-Sulfur Batteries. *Chem.—Asian J.* **2012**, *7*, 1013–1017.
32. Guo, G.; Hong, J.; Cong, C.; Zhou, X.; Zhang, K. Molybdenum Disulfide Synthesized by Hydrothermal Method as Anode for Lithium Rechargeable Batteries. *J. Mater. Sci.* **2005**, *40*, 2557–2559.
33. Zhang, C.; Wang, Z.; Guo, Z.; Lou, X. W. Synthesis of MoS_2-C One-Dimensional Nanostructures with Improved Lithium Storage Properties. *ACS Appl. Mater. Interfaces* **2012**, *4*, 3765–3768.
34. Frindt, R. F. Single Crystals of MoS_2 Several Molecular Layers Thick. *J. Appl. Phys.* **1966**, *37*, 1928.
35. Fivaz, R.; Mooser, E. Mobility of Charge Carriers in Semiconducting Layer Structures. *Phys. Rev.* **1967**, *163*, 743–755.
36. Kasowski, R. Band Structure of MoS_2 and NbS_2. *Phys. Rev. Lett.* **1973**, *30*, 1175–1178.
37. Mattheiss, L. Energy Bands for 2H-$NbSe_2$ and 2H-MoS_2. *Phys. Rev. Lett.* **1973**, *30*, 784–787.
38. Mattheiss, L. Band Structures of Transition-Metal-Dichalcogenide Layer Compounds. *Phys. Rev. B* **1973**, *8*, 3719–3740.

39. Bronsema, K. D.; De Boer, J. L.; Jellinek, F. On the Structure of Molybdenum Diselenide and Disulfide. *Z. Anorg. Allg. Chem.* **1986**, *540*, 15–17.
40. Joensen, P.; Frindt, R. F.; Morrison, S. R. Single-Layer MoS_2. *Mater. Res. Bull.* **1986**, *21*, 457–461.
41. Coehoorn, R.; Haas, C.; de Groot, R. Electronic Structure of $MoSe_2$, MoS_2, and WSe_2. II. The Nature of the Optical Band Gaps. *Phys. Rev. B* **1987**, *35*, 6203–6206.
42. Miremadi, B. K.; Cowan, T.; Morrison, S. R. New Structures from Exfoliated MoS_2. *J. Appl. Phys.* **1991**, *69*, 6373.
43. Wypych, F.; Schöllhorn, R. 1T-MoS_2, a New Metallic Modification of Molybdenum Disulfide. *J. Chem. Soc., Chem. Commun.* **1992**, 1386.
44. Byskov, L. S.; Hammer, B.; Nørskov, J. K.; Clausen, B. S.; Topsøe, H. Sulfur Bonding in MoS_2 and Co-Mo-S Structures. *Catal. Lett.* **1997**, *47*, 177–182.
45. Wypych, F.; Weber, T.; Prins, R. Scanning Tunneling Microscopic Investigation of 1T-MoS_2. *Chem. Mater.* **1998**, *10*, 723–727.
46. Helveg, S.; Lauritsen, J. V.; Laegsgaard, E.; Stensgaard, I. I.; Norskov, J. K.; Clausen, B. S.; Topsoe, H.; Besenbacher, F. Atomic-Scale Structure of Single-Layer MoS_2 Nanoclusters. *Phys. Rev. Lett.* **2000**, *84*, 951–954.
47. Böker, T.; Severin, R.; Müller, A.; Janowitz, C.; Manzke, R.; Voß, D.; Krüger, P.; Mazur, A.; Pollmann, J. Band Structure of MoS_2, $MoSe_2$, and A-$MoTe_2$: Angle-Resolved Photoelectron Spectroscopy and *Ab Initio* Calculations. *Phys. Rev. B* **2001**, *64*, 235305.
48. Lauritsen, J. V.; Kibsgaard, J.; Helveg, S.; Topsoe, H.; Clausen, B. S.; Laegsgaard, E.; Besenbacher, F. Size-Dependent Structure of MoS_2 Nanocrystals. *Nat. Nanotechnol.* **2007**, *2*, 53–58.
49. Lee, C.; Yan, H.; Brus, L. E.; Heinz, T. F.; Hone, J.; Ryu, S. Anomalous Lattice Vibrations of Single- and Few-Layer MoS_2. *ACS Nano* **2010**, *4*, 2695–2700.
50. Mak, K. F.; Lee, C.; Hone, J.; Shan, J.; Heinz, T. F. Atomically Thin MoS_2: A New Direct-Gap Semiconductor. *Phys. Rev. Lett.* **2010**, *105*, 136805.
51. Wypych, F.; Schöllhorn, R. 1T-MoS_2, a New Metallic Modification of Molybdenum Disulfide. *J. Chem. Soc., Chem. Commun.* **1992**, 1386.
52. Ramakrishna Matte, H. S. S.; Gomathi, A.; Manna, A. K.; Late, D. J.; Datta, R.; Pati, S. K.; Rao, C. N. R. MoS_2 and WS_2 Analogues of Graphene. *Angew. Chem.* **2010**, *122*, 4153–4156.
53. Zeng, H.; Dai, J.; Yao, W.; Xiao, D.; Cui, X. Valley Polarization in MoS_2 Monolayers by Optical Pumping. *Nat. Nanotechnol.* **2012**, *7*, 490–493.
54. Eda, G.; Yamaguchi, H.; Voiry, D.; Fujita, T.; Chen, M.; Chhowalla, M. Photoluminescence from Chemically Exfoliated MoS_2. *Nano Lett.* **2011**, *11*, 5111–5116.
55. Ataca, C.; Şahin, H.; Ciraci, S. Stable, Single-Layer MX_2 Transition-Metal Oxides and Dichalcogenides in a Honeycomb-like Structure. *J. Phys. Chem. C* **2012**, *116*, 8983–8999.
56. Ataca, C.; Topsakal, M.; Aktürk, E.; Ciraci, S. A Comparative Study of Lattice Dynamics of Three- and Two-Dimensional MoS_2. *J. Phys. Chem. C* **2011**, *115*, 16354–16361.
57. Castellanos-Gomez, A.; Poot, M.; Steele, G. A.; van der Zant, H. S.; Agrait, N.; Rubio-Bollinger, G. Elastic Properties of Freely Suspended MoS_2 Nanosheets. *Adv. Mater.* **2012**, *24*, 772–775.
58. Wagner, P.; Ivanovskaya, V. V.; Rayson, M. J.; Briddon, P. R.; Ewels, C. P. Mechanical Properties of Nanosheets and Nanotubes Investigated Using a New Geometry Independent Volume Definition. *J. Phys.: Condens. Matter* **2013**, *25*, 155302.
59. Li, T. Ideal Strength and Phonon Instability in Single-Layer MoS_2. *Phys. Rev. B* **2012**, *85*, 235407.
60. Bertolazzi, S.; Brivio, J.; Kis, A. Stretching and Breaking of Ultrathin MoS_2. *ACS Nano* **2011**, *5*, 9703–9709.
61. Pu, J.; Yomogida, Y.; Liu, K. K.; Li, L. J.; Iwasa, Y.; Takenobu, T. Highly Flexible MoS_2 Thin-Film Transistors with Ion Gel Dielectrics. *Nano Lett.* **2012**, *12*, 4013–4017.
62. Duerloo, K.-A. N.; Ong, M. T.; Reed, E. J. Intrinsic Piezoelectricity in Two-Dimensional Materials. *J. Phys. Chem. Lett.* **2012**, *3*, 2871–2876.
63. Wang, Z.; Lee, J.; Feng, P. X. L. Exploiting Irregular MoS_2 Nanostructures for Very High Frequency (VHF) Nanomechanical Resonators with Mode Shape Engineering and Frequency Control. *Proc. Jt. Meet. Eur. Freq. Time Forum IEEE Int. Freq. Control Symp.* **2013**, 551–554.
64. Lee, J.; Wang, Z.; He, K.; Shan, J.; Feng, P. X. High Frequency MoS_2 Nanomechanical Resonators. *ACS Nano* **2013**, *7*, 6086–6091.
65. Zhao, Y.; Luo, X.; Li, H.; Zhang, J.; Araujo, P. T.; Gan, C. K.; Wu, J.; Zhang, H.; Quek, S. Y.; Dresselhaus, M. S.; *et al.* Interlayer Breathing and Shear Modes in Few-Trilayer MoS_2 and WSe_2. *Nano Lett.* **2013**, *13*, 1007–1015.
66. Molina-Sánchez, A.; Wirtz, L. Phonons in Single-Layer and Few-Layer MoS_2 and Ws_2. *Phys. Rev. B* **2011**, *84*, 155413.
67. Sahoo, S.; Gaur, A. P. S.; Ahmadi, M.; Guinel, M. J. F.; Katiyar, R. S. Temperature-Dependent Raman Studies and Thermal Conductivity of Few-Layer MoS_2. *J. Phys. Chem. C* **2013**, *117*, 9042–9047.
68. Malard, L. M.; Alencar, T. V.; Barboza, A. P. M.; Mak, K. F.; de Paula, A. M. Observation of Intense Second Harmonic Generation from MoS_2 Atomic Crystals. *Phys. Rev. B* **2013**, *87*, 1–5.
69. Kumar, N.; Najmaei, S.; Cui, Q.; Ceballos, F.; Ajayan, P.; Lou, J.; Zhao, H. Second Harmonic Microscopy of Monolayer MoS_2. *Phys. Rev. B* **2013**, *87*, 161403.
70. Li, Y.; Rao, Y.; Mak, K. F.; You, Y.; Wang, S.; Dean, C. R.; Heinz, T. F. Probing Symmetry Properties of Few-Layer MoS_2 and H-BN by Optical Second-Harmonic Generation. *Nano Lett.* **2013**, *13*, 3329–3333.
71. Li, H.; Zhang, Q.; Yap, C. C. R.; Tay, B. K.; Edwin, T. H. T.; Olivier, A.; Baillargeat, D. From Bulk to Monolayer MoS_2: Evolution of Raman Scattering. *Adv. Funct. Mater.* **2012**, *22*, 1385–1390.
72. Chakraborty, B.; Matte, H. S. S. R.; Sood, A. K.; Rao, C. N. R. Layer-Dependent Resonant Raman Scattering of a Few Layer MoS_2. *J. Raman Spectrosc.* **2013**, *44*, 92–96.
73. Zhang, W.; Huang, J. K.; Chen, C. H.; Chang, Y. H.; Cheng, Y. J.; Li, L. J. High-Gain Phototransistors Based on a CVD MoS_2 Monolayer. *Adv. Mater.* **2013**, *25*, 3456–3461.
74. Chakraborty, B.; Bera, A.; Muthu, D. V. S.; Bhowmick, S.; Waghmare, U. V.; Sood, A. K. Symmetry-Dependent Phonon Renormalization in Monolayer MoS_2 Transistor. *Phys. Rev. B* **2012**, *85*, 161403.
75. Zeng, H.; Zhu, B.; Liu, K.; Fan, J.; Cui, X.; Zhang, Q. M. Low-Frequency Raman Modes and Electronic Excitations in Atomically Thin MoS_2 Films. *Phys. Rev. B* **2012**, *86*, 241301.
76. Plechinger, G.; Heydrich, S.; Eroms, J.; Weiss, D.; Schüller, C.; Korn, T. Raman Spectroscopy of the Interlayer Shear Mode in Few-Layer MoS_2 Flakes. *Appl. Phys. Lett.* **2012**, *101*, 101906.
77. Lanzillo, N. A.; Glen Birdwell, A.; Amani, M.; Crowne, F. J.; Shah, P. B.; Najmaei, S.; Liu, Z.; Ajayan, P. M.; Lou, J.; Dubey, M.; *et al.* Temperature-Dependent Phonon Shifts in Monolayer MoS_2. *Appl. Phys. Lett.* **2013**, *103*, 093102.
78. Najmaei, S.; Liu, Z.; Ajayan, P. M.; Lou, J. Thermal Effects on the Characteristic Raman Spectrum of Molybdenum Disulfide (MoS_2) of Varying Thicknesses. *Appl. Phys. Lett.* **2012**, *100*, 013106.
79. Wang, Y.; Cong, C.; Qiu, C.; Yu, T. Raman Spectroscopy Study of Lattice Vibration and Crystallographic Orientation of Monolayer MoS_2 under Uniaxial Strain. *Small* **2013**, *9*, 2857–2861.
80. Splendiani, A.; Sun, L.; Zhang, Y.; Li, T.; Kim, J.; Chim, C. Y.; Galli, G.; Wang, F. Emerging Photoluminescence in Monolayer MoS_2. *Nano Lett.* **2010**, *10*, 1271–1275.
81. Kadantsev, E. S.; Hawrylak, P. Electronic Structure of a Single MoS_2 Monolayer. *Solid State Commun.* **2012**, *152*, 909–913.
82. Radisavljevic, B.; Radenovic, A.; Brivio, J.; Giacometti, V.; Kis, A. Single-Layer MoS_2 Transistors. *Nat. Nanotechnol.* **2011**, *6*, 147–150.

83. Ellis, J. K.; Lucero, M. J.; Scuseria, G. E. The Indirect to Direct Band Gap Transition in Multilayered MoS_2 As Predicted by Screened Hybrid Density Functional Theory. *Appl. Phys. Lett.* **2011**, *99*, 261908.
84. Kuc, A.; Zibouche, N.; Heine, T. Influence of Quantum Confinement on the Electronic Structure of the Transition Metal Sulfide TS_2. *Phys. Rev. B* **2011**, *83*, 245213.
85. Ataca, C.; Ciraci, S. Functionalization of Single-Layer MoS_2 Honeycomb Structures. *J. Phys. Chem. C* **2011**, *115*, 13303–13311.
86. Kang, J.; Tongay, S.; Zhou, J.; Li, J.; Wu, J. Band Offsets and Heterostructures of Two-Dimensional Semiconductors. *Appl. Phys. Lett.* **2013**, *102*, 012111.
87. Zahid, F.; Liu, L.; Zhu, Y.; Wang, J.; Guo, H. A Generic Tight-Binding Model for Monolayer, Bilayer and Bulk MoS_2. *AIP Adv.* **2013**, *3*, 052111.
88. Kormányos, A.; Zólyomi, V.; Drummond, N. D.; Rakyta, P.; Burkard, G.; Fal'ko, V. I. Monolayer MoS_2: Trigonal Warping, the Γ Valley, and Spin−Orbit Coupling Effects. *Phys. Rev. B* **2013**, *88*, 045416.
89. Rostami, H.; Moghaddam, A. G.; Asgari, R. Effective Lattice Hamiltonian for Monolayer MoS_2: Tailoring Electronic Structure with Perpendicular Electric and Magnetic Fields. *Phys. Rev. B* **2013**, *88*, 085440.
90. Komsa, H.-P.; Krasheninnikov, A. V. Effects of Confinement and Environment on the Electronic Structure and Exciton Binding Energy of MoS_2 from First Principles. *Phys. Rev. B* **2012**, *86*, 241201.
91. Kumar, A.; Ahluwalia, P. K. Tunable Dielectric Response of Transition Metals Dichalcogenides MX_2 (M=Mo, W; X=S, Se, Te): Effect of Quantum Confinement. *Phys. B (Amsterdam, Neth.)* **2012**, *407*, 4627–4634.
92. Han, S. W.; Cha, G.-B.; Frantzeskakis, E.; Razado-Colambo, I.; Avila, J.; Park, Y. S.; Kim, D.; Hwang, J.; Kang, J. S.; Ryu, S.; *et al.* Band-Gap Expansion in the Surface-Localized Electronic Structure of MoS_2(0002). *Phys. Rev. B* **2012**, *86*, 115105.
93. Mahatha, S. K.; Menon, K. S. Inhomogeneous Band Bending on MoS_2(0001) Arising from Surface Steps and Dislocations. *J. Phys.: Condens. Matter* **2012**, *24*, 305502.
94. Salmani-Jelodar, M.; Tan, Y.; Klimeck, G. Single Layer MoS_2 Band Structure and Transport. *Int. Semicond. Device Res. Symp.* **2011**, *6*, 1–2.
95. Kaasbjerg, K.; Thygesen, K. S.; Jacobsen, K. W. Phonon-Limited Mobility in n-Type Single-Layer MoS_2 from First Principles. *Phys. Rev. B* **2012**, *85*, 115317.
96. Tiras, E.; Ardali, S.; Tiras, T.; Arslan, E.; Cakmakyapan, S.; Kazar, O.; Hassan, J.; Janzén, E.; Ozbay, E. Effective Mass of Electron in Monolayer Graphene: Electron−Phonon Interaction. *J. Appl. Phys.* **2013**, *113*, 043708.
97. Taniguchi, K.; Matsumoto, A.; Shimotani, H.; Takagi, H. Electric-Field-Induced Superconductivity at 9.4 K in a Layered Transition Metal Disulphide MoS_2. *Appl. Phys. Lett.* **2012**, *101*, 109902.
98. Roldán, R.; Cappelluti, E.; Guinea, F. Interactions and Superconductivity in Heavily Doped MoS_2. *Phys. Rev. B* **2013**, *88*, 1–5.
99. Ge, Y.; Liu, A. Y. Phonon-Mediated Superconductivity in Electron-Doped Single-Layer MoS_2: A First-Principles Prediction. *Phys. Rev. B* **2013**, *87*, 241408.
100. Radisavljevic, B.; Kis, A. Mobility Engineering and a Metal-Insulator Transition in Monolayer MoS_2. *Nat. Mater.* **2013**, *12*, 815–820.
101. Brivio, J.; Alexander, D. T.; Kis, A. Ripples and Layers in Ultrathin MoS_2 Membranes. *Nano Lett.* **2011**, *11*, 5148–5153.
102. Qi, J.; Li, X.; Qian, X.; Feng, J. Bandgap Engineering of Rippled MoS_2 Monolayer under External Electric Field. *Appl. Phys. Lett.* **2013**, *102*, 173112.
103. Liu, Q.; Li, L.; Li, Y.; Gao, Z.; Chen, Z.; Lu, J. Tuning Electronic Structure of Bilayer MoS_2 by Vertical Electric Field: A First-Principles Investigation. *J. Phys. Chem. C* **2012**, *116*, 21556–21562.
104. Wang, R.; Ruzicka, B. A.; Kumar, N.; Bellus, M. Z.; Chiu, H.-Y.; Zhao, H. Ultrafast and Spatially Resolved Studies of Charge Carriers in Atomically Thin Molybdenum Disulfide. *Phys. Rev. B* **2012**, *86*, 045406.
105. Jena, D.; Konar, A. Enhancement of Carrier Mobility in Semiconductor Nanostructures by Dielectric Engineering. *Phys. Rev. Lett.* **2007**, *98*, 136805.
106. Qiu, H.; Pan, L.; Yao, Z.; Li, J.; Shi, Y.; Wang, X. Electrical Characterization of Back-Gated Bi-layer MoS_2 Field-Effect Transistors and the Effect of Ambient on Their Performances. *Appl. Phys. Lett.* **2012**, *100*, 123104.
107. Mann, J.; Sun, D.; Ma, Q.; Chen, J.-R.; Preciado, E.; Ohta, T.; Diaconescu, B.; Yamaguchi, K.; Tran, T.; Wurch, M.; *et al.* Facile Growth of Monolayer MoS_2 Film Areas on SiO_2. *Eur. Phys. J. B* **2013**, *86*, 226.
108. Liu, K. K.; Zhang, W.; Lee, Y. H.; Lin, Y. C.; Chang, M. T.; Su, C. Y.; Chang, C. S.; Li, H.; Shi, Y.; Zhang, H.; *et al.* Growth of Large-Area and Highly Crystalline MoS_2 Thin Layers on Insulating Substrates. *Nano Lett.* **2012**, *12*, 1538–1544.
109. Wu, W.; De, D.; Chang, S.-C.; Wang, Y.; Peng, H.; Bao, J.; Pei, S.-S. High Mobility and High on/Off Ratio Field-Effect Transistors Based on Chemical Vapor Deposited Single-Crystal MoS_2 Grains. *Appl. Phys. Lett.* **2013**, *102*, 142106.
110. Das, S.; Chen, H. Y.; Penumatcha, A. V.; Appenzeller, J. High Performance Multilayer MoS_2 Transistors with Scandium Contacts. *Nano Lett.* **2013**, *13*, 100–105.
111. Laskar, M. R.; Ma, L.; Kannappan, S.; Sung Park, P.; Krishnamoorthy, S.; Nath, D. N.; Lu, W.; Wu, Y.; Rajan, S. Large Area Single Crystal (0001) Oriented MoS_2. *Appl. Phys. Lett.* **2013**, *102*, 252108.
112. Lin, M.-W.; Liu, L.; Lan, Q.; Tan, X.; Dhindsa, K. S.; Zeng, P.; Naik, V. M.; Cheng, M. M.-C.; Zhou, Z. Mobility Enhancement and Highly Efficient Gating of Monolayer MoS_2 Transistors with Polymer Electrolyte. *J. Phys. D: Appl. Phys.* **2012**, *45*, 345102.
113. Min, S. W.; Lee, H. S.; Choi, H. J.; Park, M. K.; Nam, T.; Kim, H.; Ryu, S.; Im, S. Nanosheet Thickness-Modulated MoS_2 Dielectric Property Evidenced by Field-Effect Transistor Performance. *Nanoscale* **2013**, *5*, 548–551.
114. Lee, Y. H.; Zhang, X. Q.; Zhang, W.; Chang, M. T.; Lin, C. T.; Chang, K. D.; Yu, Y. C.; Wang, J. T.; Chang, C. S.; Li, L. J.; *et al.* Synthesis of Large-Area MoS_2 Atomic Layers with Chemical Vapor Deposition. *Adv. Mater.* **2012**, *24*, 2320–2325.
115. Najmaei, S.; Liu, Z.; Zhou, W.; Zou, X.; Shi, G.; Lei, S.; Yakobson, B. I.; Idrobo, J. C.; Ajayan, P. M.; Lou, J. Vapour Phase Growth and Grain Boundary Structure of Molybdenum Disulphide Atomic Layers. *Nat. Mater.* **2013**, *12*, 754–759.
116. Lin, Y. C.; Zhang, W.; Huang, J. K.; Liu, K. K.; Lee, Y. H.; Liang, C. T.; Chu, C. W.; Li, L. J. Wafer-Scale MoS_2 Thin Layers Prepared by MoO_3 Sulfurization. *Nanoscale* **2012**, *4*, 6637–6641.
117. Zhan, Y.; Liu, Z.; Najmaei, S.; Ajayan, P. M.; Lou, J. Large-Area Vapor-Phase Growth and Characterization of MoS_2 Atomic Layers on a SiO_2 Substrate. *Small* **2012**, *8*, 966–971.
118. Nam, H.; Wi, S.; Rokni, H.; Chen, M.; Priessnitz, G.; Lu, W.; Liang, X. MoS_2 Transistors Fabricated *via* Plasma-Assisted Nanoprinting of Few-Layer MoS_2 Flakes into Large-Area Arrays. *ACS Nano* **2013**, *7*, 5870–5881.
119. Zhang, Y.; Ye, J.; Matsuhashi, Y.; Iwasa, Y. Ambipolar MoS_2 Thin Flake Transistors. *Nano Lett.* **2012**, *12*, 1136–1140.
120. Bao, W.; Cai, X.; Kim, D.; Sridhara, K.; Fuhrer, M. S. High Mobility Ambipolar MoS_2 Field-Effect Transistors: Substrate and Dielectric Effects. *Appl. Phys. Lett.* **2013**, *102*, 042104.
121. Perera, M. M.; Lin, M. W.; Chuang, H. J.; Chamlagain, B. P.; Wang, C.; Tan, X.; Cheng, M. M.; Tomanek, D.; Zhou, Z. Improved Carrier Mobility in Few-Layer MoS_2 Field-Effect Transistors with Ionic-Liquid Gating. *ACS Nano* **2013**, *7*, 4449–4458.
122. Dolui, K.; Rungger, I.; Sanvito, S. Origin of the n-Type and p-Type Conductivity of MoS_2 Monolayers on a SiO_2 Substrate. *Phys. Rev. B* **2013**, *87*, 165402.
123. Peelaers, H.; Van de Walle, C. G. Effects of Strain on Band Structure and Effective Masses in MoS_2. *Phys. Rev. B* **2012**, *86*, 241401.

124. Shi, H.; Pan, H.; Zhang, Y.-W.; Yakobson, B. Quasiparticle Band Structures and Optical Properties of Strained Monolayer MoS_2 and WS_2. *Phys. Rev. B* **2013**, *87*, 155304.
125. Conley, H. J.; Wang, B.; Ziegler, J. I.; Haglund, R. F., Jr.; Pantelides, S. T.; Bolotin, K. I. Bandgap Engineering of Strained Monolayer and Bilayer MoS_2. *Nano Lett.* **2013**, *13*, 3626–3630.
126. Mohammad Tabatabaei, S.; Noei, M.; Khaliji, K.; Pourfath, M.; Fathipour, M. A First-Principles Study on the Effect of Biaxial Strain on the Ultimate Performance of Monolayer MoS_2-Based Double Gate Field Effect Transistor. *J. Appl. Phys.* **2013**, *113*, 163708.
127. Hui, Y. Y.; Liu, X.; Jie, W.; Chan, N. Y.; Hao, J.; Hsu, Y. T.; Li, L. J.; Guo, W.; Lau, S. P. Exceptional Tunability of Band Energy in a Compressively Strained Trilayer MoS_2 Sheet. *ACS Nano* **2013**, *7*, 7126–7131.
128. He, K.; Poole, C.; Mak, K. F.; Shan, J. Experimental Demonstration of Continuous Electronic Structure Tuning *via* Strain in Atomically Thin MoS_2. *Nano Lett.* **2013**, *13*, 2931–2936.
129. Castellanos-Gomez, A.; Roldan, R.; Cappelluti, E.; Buscema, M.; Guinea, F.; van der Zant, H. S.; Steele, G. A. Local Strain Engineering in Atomically Thin MoS_2. *Nano Lett.* **2013**, *13*, 5361–5366.
130. Zhu, C. R.; Wang, G.; Liu, B. L.; Marie, X.; Qiao, X. F.; Zhang, X.; Wu, X. X.; Fan, H.; Tan, P. H.; Amand, T.; *et al.* Strain Tuning of Optical Emission Energy and Polarization in Monolayer and Bilayer MoS_2. *Phys. Rev. B* **2013**, *88*, 1–5.
131. Komsa, H.-P.; Krasheninnikov, A. V. Two-Dimensional Transition Metal Dichalcogenide Alloys: Stability and Electronic Properties. *J. Phys. Chem. Lett.* **2012**, *3*, 3652–3656.
132. Chen, Y.; Xi, J.; Dumcenco, D. O.; Liu, Z.; Suenaga, K.; Wang, D.; Shuai, Z.; Huang, Y. S.; Xie, L. Tunable Band Gap Photoluminescence from Atomically Thin Transition-Metal Dichalcogenide Alloys. *ACS Nano* **2013**, *7*, 4610–4616.
133. Huang, Z.; He, C.; Qi, X.; Yang, H.; Liu, W.; Wei, X.; Peng, X.; Zhong, J. Band Structure Engineering of Monolayer MoS_2 on H-BN: First-Principles Calculations. *J. Phys. D: Appl. Phys.* **2014**, *47*, 075301.
134. Tsai, D. S.; Liu, K. K.; Lien, D. H.; Tsai, M. L.; Kang, C. F.; Lin, C. A.; Li, L. J.; He, J. H. Few-Layer MoS_2 with High Broadband Photogain and Fast Optical Switching for Use in Harsh Environments. *ACS Nano* **2013**, *7*, 3905–3911.
135. van der Zande, A.; Hone, J. Optical Materials: Inspired by Strain. *Nat. Photonics* **2012**, *6*, 804–806.
136. Gaur, A. P. S.; Sahoo, S.; Ahmadi, M.; Guinel, M. J. F.; Gupta, S. K.; Pandey, R.; Dey, S. K.; Katiyar, R. S. Optical and Vibrational Studies of Partially Edge-Terminated Vertically Aligned Nanocrystalline MoS_2 thin Films. *J. Phys. Chem. C* **2013**, *117*, 26262–26268.
137. Schuller, J. A.; Karaveli, S.; Schiros, T.; He, K.; Yang, S.; Kymissis, I.; Shan, J.; Zia, R. Orientation of Luminescent Excitons in Layered Nanomaterials. *Nat. Nanotechnol.* **2013**, *8*, 271–276.
138. Sallen, G.; Bouet, L.; Marie, X.; Wang, G.; Zhu, C. R.; Han, W. P.; Lu, Y.; Tan, P. H.; Amand, T.; Liu, B. L.; *et al.* Robust Optical Emission Polarization in MoS_2 Monolayers through Selective Valley Excitation. *Phys. Rev. B* **2012**, *86*, 081301.
139. Alkis, S.; Oztas, T.; Aygun, L. E.; Bozkurt, F.; Okyay, A. K.; Ortac, B. Thin Film MoS_2 Nanocrystal Based Ultraviolet Photodetector. *Opt. Express* **2012**, *20*, 21815–21820.
140. Mak, K. F.; He, K.; Lee, C.; Lee, G. H.; Hone, J.; Heinz, T. F.; Shan, J. Tightly Bound Trions in Monolayer MoS_2. *Nat. Mater.* **2013**, *12*, 207–211.
141. Balendhran, S.; Ou, J. Z.; Bhaskaran, M.; Sriram, S.; Ippolito, S.; Vasic, Z.; Kats, E.; Bhargava, S.; Zhuiykov, S.; Kalantar-Zadeh, K. Atomically Thin Layers of MoS_2 *via* a Two Step Thermal Evaporation-Exfoliation Method. *Nanoscale* **2012**, *4*, 461–466.
142. Ji, Q.; Zhang, Y.; Gao, T.; Zhang, Y.; Ma, D.; Liu, M.; Chen, Y.; Qiao, X.; Tan, P. H.; Kan, M.; *et al.* Epitaxial Monolayer MoS_2 on Mica with Novel Photoluminescence. *Nano Lett.* **2013**, *13*, 3870–3877.
143. Shi, Y.; Zhou, W.; Lu, A. Y.; Fang, W.; Lee, Y. H.; Hsu, A. L.; Kim, S. M.; Kim, K. K.; Yang, H. Y.; Li, L. J.; *et al.* van der Waals Epitaxy of MoS_2 Layers Using Graphene as Growth Templates. *Nano Lett.* **2012**, *12*, 2784–2791.
144. Wu, S.; Huang, C.; Aivazian, G.; Ross, J. S.; Cobden, D. H.; Xu, X. Vapor–Solid Growth of High Optical Quality MoS_2 Monolayers with Near-Unity Valley Polarization. *ACS Nano* **2013**, *7*, 2768–2772.
145. Sercombe, D.; Schwarz, S.; Del Pozo-Zamudio, O.; Liu, F.; Robinson, B. J.; Chekhovich, E. A.; Tartakovskii, I. I.; Kolosov, O.; Tartakovskii, A. I. Optical Investigation of the Natural Electron Doping in Thin MoS_2 Films Deposited on Dielectric Substrates. *Sci. Rep.* **2013**, *3*, 3489.
146. Soklaski, R.; Liang, Y.; Zhang, C.; Wang, H.; Rana, F.; Yang, L. Temperature Renormalization of Optical Spectra of Monolayer MoS_2. *arXiv:1401.5732v1* **2014**, 5732.
147. Tongay, S.; Zhou, J.; Ataca, C.; Liu, J.; Kang, J. S.; Matthews, T. S.; You, L.; Li, J.; Grossman, J. C.; Wu, J. Broad-Range Modulation of Light Emission in Two-Dimensional Semiconductors by Molecular Physisorption Gating. *Nano Lett.* **2013**, *13*, 2831–2836.
148. Buscema, M.; Barkelid, M.; Zwiller, V.; van der Zant, H. S.; Steele, G. A.; Castellanos-Gomez, A. Large and Tunable Photothermoelectric Effect in Single-Layer MoS_2. *Nano Lett.* **2013**, *13*, 358–363.
149. Ramasubramaniam, A. Large Excitonic Effects in Monolayers of Molybdenum and Tungsten Dichalcogenides. *Phys. Rev. B* **2012**, *86*, 115409.
150. Stébé, B.; Ainane, A. Ground State Energy and Optical Absorption of Excitonic Trions in Two Dimensional Semiconductors. *Superlattices Microstruct.* **1989**, *5*, 545–548.
151. Combescot, M.; Betbeder-Matibet, O.; Dubin, F. The Trion: Two Electrons Plus One Hole *versus* One Electron Plus One Exciton. *Eur. Phys. J. B* **2004**, *42*, 63–83.
152. Feng, J.; Qian, X.; Huang, C.-W.; Li, J. Strain-Engineered Artificial Atom as a Broad-Spectrum Solar Energy Funnel. *Nat. Photonics* **2012**, *6*, 866–872.
153. Cao, T.; Wang, G.; Han, W.; Ye, H.; Zhu, C.; Shi, J.; Niu, Q.; Tan, P.; Wang, E.; Liu, B.; *et al.* Valley-Selective Circular Dichroism of Monolayer Molybdenum Disulphide. *Nat. Commun.* **2012**, *3*, 887.
154. Nebel, C. E. Valleytronics: Electrons Dance in Diamond. *Nat. Mater.* **2013**, *12*, 690–691.
155. Wolf, S. A.; Awschalom, D. D.; Buhrman, R. A.; Daughton, J. M.; von Molnar, S.; Roukes, M. L.; Chtchelkanova, A. Y.; Treger, D. M. Spintronics: A Spin-Based Electronics Vision for the Future. *Science* **2001**, *294*, 1488–1495.
156. Zhu, Z. Y.; Cheng, Y. C.; Schwingenschlögl, U. Giant Spin–Orbit-Induced Spin Splitting in Two-Dimensional Transition-Metal Dichalcogenide Semiconductors. *Phys. Rev. B* **2011**, *84*, 153402.
157. Bishnoi, B.; Ghosh, B. Spin Transport in Monolayer Molybdenum Disulfide (MoS_2). *J. Comput. Electron.* **2013**, 10.1007/s10825-013-0547-7.
158. Mak, K. F.; He, K.; Shan, J.; Heinz, T. F. Control of Valley Polarization in Monolayer MoS_2 by Optical Helicity. *Nat. Nanotechnol.* **2012**, *7*, 494–498.
159. Xiao, D.; Liu, G.-B.; Feng, W.; Xu, X.; Yao, W. Coupled Spin and Valley Physics in Monolayers of MoS_2 and Other Group-VI Dichalcogenides. *Phys. Rev. Lett.* **2012**, *108*, 1–5.
160. Lu, H. Z.; Yao, W.; Xiao, D.; Shen, S. Q. Intervalley Scattering and Localization Behaviors of Spin-Valley Coupled Dirac Fermions. *Phys. Rev. Lett.* **2013**, *110*, 016806.
161. Li, Z.; Carbotte, J. P. Impact of Electron–Phonon Interaction on Dynamic Conductivity of Gapped Dirac Fermions: Application to Single Layer MoS_2. *Phys. B (Amsterdam, Neth.)* **2013**, *421*, 97–104.
162. Li, Z.; Carbotte, J. P. Longitudinal and Spin-Valley Hall Optical Conductivity in Single Layer MoS_2. *Phys. Rev. B* **2012**, *86*, 205425.
163. Wu, S.; Ross, J. S.; Liu, G.-B.; Aivazian, G.; Jones, A.; Fei, Z.; Zhu, W.; Xiao, D.; Yao, W.; Cobden, D.; *et al.* Electrical Tuning of Valley Magnetic Moment through Symmetry Control in Bilayer MoS_2. *Nat. Phys.* **2013**, *9*, 149–153.

164. Tongay, S.; Varnoosfaderani, S. S.; Appleton, B. R.; Wu, J.; Hebard, A. F. Magnetic Properties of MoS_2: Existence of Ferromagnetism. *Appl. Phys. Lett.* **2012**, *101*, 123105.
165. Gao, D.; Si, M.; Li, J.; Zhang, J.; Zhang, Z.; Yang, Z.; Xue, D. Ferromagnetism in Freestanding MoS_2 Nanosheets. *Nanoscale Res. Lett.* **2013**, *8*, 129.
166. Li, Y.; Zhou, Z.; Zhang, S.; Chen, Z. MoS_2 Nanoribbons: High Stability and Unusual Electronic and Magnetic Properties. *J. Am. Chem. Soc.* **2008**, *130*, 16739–16744.
167. Zhou, W.; Zou, X.; Najmaei, S.; Liu, Z.; Shi, Y.; Kong, J.; Lou, J.; Ajayan, P. M.; Yakobson, B. I.; Idrobo, J. C. Intrinsic Structural Defects in Monolayer Molybdenum Disulfide. *Nano Lett.* **2013**, *13*, 2615–2622.
168. Mathew, S.; Gopinadhan, K.; Chan, T. K.; Yu, X. J.; Zhan, D.; Cao, L.; Rusydi, A.; Breese, M. B. H.; Dhar, S.; Shen, Z. X.; *et al.* Magnetism in MoS_2 Induced by Proton Irradiation. *Appl. Phys. Lett.* **2012**, *101*, 102103.
169. Ramasubramaniam, A.; Naveh, D. Mn-Doped Monolayer MoS_2: An Atomically Thin Dilute Magnetic Semiconductor. *Phys. Rev. B* **2013**, *87*, 195201.
170. Li, H.; Lu, G.; Yin, Z.; He, Q.; Li, H.; Zhang, Q.; Zhang, H. Optical Identification of Single- and Few-Layer MoS_2 Sheets. *Small* **2012**, *8*, 682–686.
171. Late, D. J.; Liu, B.; Matte, H. S. S. R.; Rao, C. N. R.; Dravid, V. P. Rapid Characterization of Ultrathin Layers of Chalcogenides on SiO_2/Si Substrates. *Adv. Funct. Mater.* **2012**, *22*, 1894–1905.
172. Wang, Y. Y.; Gao, R. X.; Ni, Z. H.; He, H.; Guo, S. P.; Yang, H. P.; Cong, C. X.; Yu, T. Thickness Identification of Two-Dimensional Materials by Optical Imaging. *Nanotechnology* **2012**, *23*, 495713.
173. Benameur, M. M.; Radisavljevic, B.; Heron, J. S.; Sahoo, S.; Berger, H.; Kis, A. Visibility of Dichalcogenide Nanolayers. *Nanotechnology* **2011**, *22*, 125706.
174. Liu, H.; Neal, A. T.; Ye, P. D. Channel Length Scaling of MoS_2 MOSFETs. *ACS Nano* **2012**, *6*, 8563–8569.
175. Late, D. J.; Liu, B.; Matte, H. S.; Dravid, V. P.; Rao, C. N. Hysteresis in Single-Layer MoS_2 Field Effect Transistors. *ACS Nano* **2012**, *6*, 5635–5641.
176. Lee, H. S.; Min, S. W.; Park, M. K.; Lee, Y. T.; Jeon, P. J.; Kim, J. H.; Ryu, S.; Im, S. MoS_2 Nanosheets for Top-Gate Nonvolatile Memory Transistor Channel. *Small* **2012**, *8*, 3111–3115.
177. Yin, Z.; Li, H.; Li, H.; Jiang, L.; Shi, Y.; Sun, Y.; Lu, G.; Zhang, Q.; Chen, X.; Zhang, H. Single-Layer MoS_2 Phototransistors. *ACS Nano* **2012**, *6*, 74–80.
178. O'Neill, A.; Khan, U.; Coleman, J. N. Preparation of High Concentration Dispersions of Exfoliated MoS_2 with Increased Flake Size. *Chem. Mater.* **2012**, *24*, 2414–2421.
179. Zeng, Z.; Yin, Z.; Huang, X.; Li, H.; He, Q.; Lu, G.; Boey, F.; Zhang, H. Single-Layer Semiconducting Nanosheets: High-Yield Preparation and Device Fabrication. *Angew. Chem., Int. Ed.* **2011**, *50*, 11093–11097.
180. Gacem, K.; Boukhicha, M.; Chen, Z.; Shukla, A. High Quality 2d Crystals Made by Anodic Bonding: A General Technique for Layered Materials. *Nanotechnology* **2012**, *23*, 505709.
181. Dines, M. B. Intercalation in Layered Compounds. *J. Chem. Educ.* **1974**, *51*, 221.
182. Coleman, J. N.; Lotya, M.; O'Neill, A.; Bergin, S. D.; King, P. J.; Khan, U.; Young, K.; Gaucher, A.; De, S.; Smith, R. J.; *et al.* Two-Dimensional Nanosheets Produced by Liquid Exfoliation of Layered Materials. *Science* **2011**, *331*, 568–571.
183. Smith, R. J.; King, P. J.; Lotya, M.; Wirtz, C.; Khan, U.; De, S.; O'Neill, A.; Duesberg, G. S.; Grunlan, J. C.; Moriarty, G.; *et al.* Large-Scale Exfoliation of Inorganic Layered Compounds in Aqueous Surfactant Solutions. *Adv. Mater.* **2011**, *23*, 3944–3948.
184. Yao, Y.; Lin, Z.; Li, Z.; Song, X.; Moon, K.-S.; Wong, C.-p. Large-Scale Production of Two-Dimensional Nanosheets. *J. Mater. Chem.* **2012**, *22*, 13494.
185. King, L. A.; Zhao, W.; Chhowalla, M.; Riley, D. J.; Eda, G. Photoelectrochemical Properties of Chemically Exfoliated MoS_2. *J. Mater. Chem. A* **2013**, *1*, 8935.
186. Liu, J.; Zeng, Z.; Cao, X.; Lu, G.; Wang, L. H.; Fan, Q. L.; Huang, W.; Zhang, H. Preparation of MoS_2-Polyvinylpyrrolidone Nanocomposites for Flexible Nonvolatile Rewritable Memory Devices with Reduced Graphene Oxide Electrodes. *Small* **2012**, 3517–3522.
187. Castellanos-Gomez, A.; Barkelid, M.; Goossens, A. M.; Calado, V. E.; van der Zant, H. S.; Steele, G. A. Laser-Thinning of MoS_2: On Demand Generation of a Single-Layer Semiconductor. *Nano Lett.* **2012**, *12*, 3187–3192.
188. Lu, X.; Utama, M. I.; Zhang, J.; Zhao, Y.; Xiong, Q. Layer-by-Layer Thinning of MoS_2 by Thermal Annealing. *Nanoscale* **2013**, *5*, 8904–8908.
189. Liu, Y.; Nan, H.; Wu, X.; Pan, W.; Wang, W.; Bai, J.; Zhao, W.; Sun, L.; Wang, X.; Ni, Z. Layer-by-Layer Thinning of MoS_2 by Plasma. *ACS Nano* **2013**, *7*, 4202–4209.
190. Kong, D.; Wang, H.; Cha, J. J.; Pasta, M.; Koski, K. J.; Yao, J.; Cui, Y. Synthesis of MoS_2 and $MoSe_2$ Films with Vertically Aligned Layers. *Nano Lett.* **2013**, *13*, 1341–1347.
191. Yu, Y.; Li, C.; Liu, Y.; Su, L.; Zhang, Y.; Cao, L. Controlled Scalable Synthesis of Uniform, High-Quality Monolayer and Few-Layer MoS_2 Films. *Sci. Rep.* **2013**, *3*, 1866.
192. Zou, X.; Liu, Y.; Yakobson, B. I. Predicting Dislocations and Grain Boundaries in Two-Dimensional Metal-Disulfides from the First Principles. *Nano Lett.* **2013**, *13*, 253–258.
193. Le, D.; Rahman, T. S. Joined Edges in MoS_2: Metallic and Half-Metallic Wires. *J. Phys.: Condens. Matter* **2013**, *25*, 312201.
194. Ivanovskaya, V.; Zobelli, A.; Gloter, A.; Brun, N.; Serin, V.; Colliex, C. *Ab Initio* Study of Bilateral Doping within the MoS_2—NbS_2 System. *Phys. Rev. B* **2008**, *78*, 134104.
195. Dolui, K.; Rungger, I.; Das Pemmaraju, C.; Sanvito, S. Possible Doping Strategies for MoS_2 Monolayers: An *Ab Initio* Study. *Phys. Rev. B* **2013**, *88*, 1–9.
196. Chang, J.; Larentis, S.; Tutuc, E.; Register, L. F.; Banerjee, S. K. Atomistic Simulation of Doping by Adatoms in Monolayer MoS_2. *arXiv:1305.7162v2* **2013**, 7162.
197. Noh, J.-Y.; Park, M.; Kim, Y.-S.; Kim, H. Stability and Dopability of Native Defects and Group-V and -VII Impurities in Single-Layer MoS_2. *arXiv:1307.3813v1* **2013**, 3813.
198. Sun, Q.-Q.; Li, Y.-J.; He, J.-L.; Yang, W.; Zhou, P.; Lu, H.-L.; Ding, S.-J.; Wei Zhang, D. The Physics and Backward Diode Behavior of Heavily Doped Single Layer MoS_2 Based p-n Junctions. *Appl. Phys. Lett.* **2013**, *102*, 093104.
199. Chang, J.; Register, L. F.; Banerjee, S. K. Atomistic Full-Band Simulations of Monolayer MoS_2 Transistors. *Appl. Phys. Lett.* **2013**, *103*, 223509.
200. Fang, H.; Tosun, M.; Seol, G.; Chang, T. C.; Takei, K.; Guo, J.; Javey, A. Degenerate N-Doping of Few-Layer Transition Metal Dichalcogenides by Potassium. *Nano Lett.* **2013**, *13*, 1991–1995.
201. Yoon, Y.; Ganapathi, K.; Salahuddin, S. How Good Can Monolayer MoS_2 Transistors Be? *Nano Lett.* **2011**, *11*, 3768–3773.
202. Alam, K.; Lake, R. Monolayer MoS_2 Transistors Beyond the Technology Road Map. *IEEE Trans. Electron Devices* **2012**, *59*, 3250–3254.
203. Lembke, D.; Kis, A. Breakdown of High-Performance Monolayer MoS_2 Transistors. *ACS Nano* **2012**, *6*, 10070–10075.
204. Liu, H.; Gu, J.; Ye, P. D. Nanoribbon Transistors: Transition from Depletion Mode to Enhancement Mode by Channel-Width Trimming. *IEEE Electron Device Lett.* **2012**, *33*, 1273–1275.
205. Liu, L.; Kumar, S. B.; Ouyang, Y.; Guo, J. Performance Limits of Monolayer Transition Metal Dichalcogenide Transistors. *IEEE Trans. Electron Devices* **2011**, *58*, 3042–3047.
206. Das, S.; Appenzeller, J. Where Does the Current Flow in Two-Dimensional Layered Systems? *Nano Lett.* **2013**, *13*, 3396–3402.
207. Jariwala, D.; Sangwan, V. K.; Late, D. J.; Johns, J. E.; Dravid, V. P.; Marks, T. J.; Lauhon, L. J.; Hersam, M. C. Band-like Transport in High Mobility Unencapsulated Single-Layer MoS_2 Transistors. *Appl. Phys. Lett.* **2013**, *102*, 173107.
208. Popov, I.; Seifert, G.; Tomanek, D. Designing Electrical Contacts to MoS_2 Monolayers: A Computational Study. *Phys. Rev. Lett.* **2012**, *108*, 156802.

209. Kim, S.; Konar, A.; Hwang, W. S.; Lee, J. H.; Lee, J.; Yang, J.; Jung, C.; Kim, H.; Yoo, J. B.; Choi, J. Y.; *et al.* High-Mobility and Low-Power Thin-Film Transistors Based on Multilayer MoS_2 Crystals. *Nat. Commun.* **2012**, *3*, 1011.
210. Chang, H. Y.; Yang, S.; Lee, J.; Tao, L.; Hwang, W. S.; Jena, D.; Lu, N.; Akinwande, D. High-Performance, Highly Bendable MoS_2 Transistors with High-K Dielectrics for Flexible Low-Power Systems. *ACS Nano* **2013**, *7*, 5446–5452.
211. Liu, H.; Ye, P. D. MoS_2 Dual-Gate Mosfet with Atomic-Layer-Deposited Al_2O_3 as Top-Gate Dielectric. *IEEE Electron Device Lett.* **2012**, *33*, 546–548.
212. Chan, M. Y.; Komatsu, K.; Li, S. L.; Xu, Y.; Darmawan, P.; Kuramochi, H.; Nakaharai, S.; Aparecido-Ferreira, A.; Watanabe, K.; Taniguchi, T.; *et al.* Suppression of Thermally Activated Carrier Transport in Atomically Thin MoS_2 on Crystalline Hexagonal Boron Nitride Substrates. *Nanoscale* **2013**, *5*, 9572–9576.
213. Bertolazzi, S.; Krasnozhon, D.; Kis, A. Nonvolatile Memory Cells Based on MoS_2/Graphene Heterostructures. *ACS Nano* **2013**, *7*, 3246–3252.
214. Radisavljevic, B.; Whitwick, M. B.; Kis, A. Integrated Circuits and Logic Operations Based on Single-Layer MoS_2. *ACS Nano* **2011**, *5*, 9934–9938.
215. Wang, H.; Yu, L.; Lee, Y. H.; Shi, Y.; Hsu, A.; Chin, M. L.; Li, L. J.; Dubey, M.; Kong, J.; Palacios, T. Integrated Circuits Based on Bilayer MoS_2 Transistors. *Nano Lett.* **2012**, *12*, 4674–4680.
216. Ma, Y.; Dai, Y.; Guo, M.; Niu, C.; Huang, B. Graphene Adhesion on MoS_2 Monolayer: An *Ab Initio* Study. *Nanoscale* **2011**, *3*, 3883–3887.
217. Huang, J.; Somu, S.; Busnaina, A. A Molybdenum Disulfide/Carbon Nanotube Heterogeneous Complementary Inverter. *Nanotechnology* **2012**, *23*, 335203.
218. Lee, H. S.; Min, S. W.; Chang, Y. G.; Park, M. K.; Nam, T.; Kim, H.; Kim, J. H.; Ryu, S.; Im, S. MoS_2 Nanosheet Phototransistors with Thickness-Modulated Optical Energy Gap. *Nano Lett.* **2012**, *12*, 3695–3700.
219. Choi, W.; Cho, M. Y.; Konar, A.; Lee, J. H.; Cha, G. B.; Hong, S. C.; Kim, S.; Kim, J.; Jena, D.; Joo, J.; *et al.* High-Detectivity Multilayer MoS_2 Phototransistors with Spectral Response from Ultraviolet to Infrared. *Adv. Mater.* **2012**, *24*, 5832–5836.
220. Lopez-Sanchez, O.; Lembke, D.; Kayci, M.; Radenovic, A.; Kis, A. Ultrasensitive Photodetectors Based on Monolayer MoS_2. *Nat. Nanotechnol.* **2013**, *8*, 497–501.
221. Zhang, W.; Chuu, C. P.; Huang, J. K.; Chen, C. H.; Tsai, M. L.; Chang, Y. H.; Liang, C. T.; Chen, Y. Z.; Chueh, Y. L.; He, J. H.; *et al.* Ultrahigh-Gain Photodetectors Based on Atomically Thin Graphene-MoS_2 Heterostructures. *Sci. Rep.* **2014**, *4*, 3826.
222. Yu, W. J.; Liu, Y.; Zhou, H.; Yin, A.; Li, Z.; Huang, Y.; Duan, X. Highly Efficient Gate-Tunable Photocurrent Generation in Vertical Heterostructures of Layered Materials. *Nat. Nanotechnol.* **2013**, *8*, 952–958.
223. Hamm, J. M.; Hess, O. Physics. Two Two-Dimensional Materials Are Better Than One. *Science* **2013**, *340*, 1298–1299.
224. Britnell, L.; Gorbachev, R. V.; Jalil, R.; Belle, B. D.; Schedin, F.; Mishchenko, A.; Georgiou, T.; Katsnelson, M. I.; Eaves, L.; Morozov, S. V.; *et al.* Field-Effect Tunneling Transistor Based on Vertical Graphene Heterostructures. *Science* **2012**, *335*, 947–950.
225. Myoung, N.; Seo, K.; Lee, S. J.; Ihm, G. Large Current Modulation and Spin-Dependent Tunneling of Vertical Graphene/MoS_2 Heterostructures. *ACS Nano* **2013**, *7*, 7021–7027.
226. Bala Kumar, S.; Seol, G.; Guo, J. Modeling of a Vertical Tunneling Graphene Heterojunction Field-Effect Transistor. *Appl. Phys. Lett.* **2012**, *101*, 033503.
227. Roy, K.; Padmanabhan, M.; Goswami, S.; Sai, T. P.; Ramalingam, G.; Raghavan, S.; Ghosh, A. Graphene-MoS_2 Hybrid Structures for Multifunctional Photoresponsive Memory Devices. *Nat. Nanotechnol.* **2013**, *8*, 826–830.
228. Keong Koh, E. W.; Chiu, C. H.; Lim, Y. K.; Zhang, Y.-W.; Pan, H. Hydrogen Adsorption on and Diffusion through MoS_2 Monolayer: First-Principles Study. *Int. J. Hydrogen Energy* **2012**, *37*, 14323–14328.
229. Yue, Q.; Shao, Z.; Chang, S.; Li, J. Adsorption of Gas Molecules on Monolayer MoS_2 and Effect of Applied Electric Field. *Nanoscale Res. Lett.* **2013**, *8*, 425.
230. Cantalini, C.; Giancaterini, L.; Donarelli, M. NO_2 Response to Few-Layers MoS_2. *Tagungsband* **2012**, 1656–1659.
231. He, Q.; Zeng, Z.; Yin, Z.; Li, H.; Wu, S.; Huang, X.; Zhang, H. Fabrication of Flexible MoS_2 Thin-Film Transistor Arrays for Practical Gas-Sensing Applications. *Small* **2012**, *8*, 2994–2999.
232. Li, H.; Yin, Z.; He, Q.; Li, H.; Huang, X.; Lu, G.; Fam, D. W.; Tok, A. I.; Zhang, Q.; Zhang, H. Fabrication of Single- and Multilayer MoS_2 Film-Based Field-Effect Transistors for Sensing NO at Room Temperature. *Small* **2012**, *8*, 63–67.
233. Late, D. J.; Huang, Y. K.; Liu, B.; Acharya, J.; Shirodkar, S. N.; Luo, J.; Yan, A.; Charles, D.; Waghmare, U. V.; Dravid, V. P.; *et al.* Sensing Behavior of Atomically Thin-Layered MoS_2 Transistors. *ACS Nano* **2013**, *7*, 4879–4891.
234. Perkins, F. K.; Friedman, A. L.; Cobas, E.; Campbell, P. M.; Jernigan, G. G.; Jonker, B. T. Chemical Vapor Sensing with Monolayer MoS_2. *Nano Lett.* **2013**, *13*, 668–673.
235. Ataca, C.; Sahin, H.; Aktürk, E.; Ciraci, S. Mechanical and Electronic Properties of MoS_2 Nanoribbons and Their Defects. *J. Phys. Chem. C* **2011**, *115*, 3934–3941.
236. Kou, L.; Tang, C.; Zhang, Y.; Heine, T.; Chen, C.; Frauenheim, T. Tuning Magnetism and Electronic Phase Transitions by Strain and Electric Field in Zigzag MoS_2 Nanoribbons. *J. Phys. Chem. Lett.* **2012**, *3*, 2934–2941.
237. Shidpour, R.; Manteghian, M. A Density Functional Study of Strong Local Magnetism Creation on MoS_2 Nanoribbon by Sulfur Vacancy. *Nanoscale* **2010**, *2*, 1429–1435.
238. Yue, Q.; Chang, S.; Kang, J.; Zhang, X.; Shao, Z.; Qin, S.; Li, J. Bandgap Tuning in Armchair MoS_2 Nanoribbon. *J. Phys.: Condens. Matter* **2012**, *24*, 335501.
239. Dolui, K.; Pemmaraju, C. D.; Sanvito, S. Electric Field Effects on Armchair MoS_2 Nanoribbons. *ACS Nano* **2012**, *6*, 4823–4834.
240. Hsu, W. K.; Chang, B. H.; Zhu, Y. Q.; Han, W. Q.; Terrones, H.; Terrones, M.; Grobert, N.; Cheetham, A. K.; Kroto, H. W.; Walton, D. R. M. An Alternative Route to Molybdenum Disulfide Nanotubes. *J. Am. Chem. Soc.* **2000**, *122*, 10155–10158.
241. Remskar, M.; Mrzel, A.; Skraba, Z.; Jesih, A.; Ceh, M.; Demsar, J.; Stadelmann, P.; Levy, F.; Mihailovic, D. Self-Assembly of Subnanometer-Diameter Single-Wall MoS_2 Nanotubes. *Science* **2001**, *292*, 479–481.
242. Visic, B.; Dominko, R.; Gunde, M. K.; Hauptman, N.; Skapin, S. D.; Remskar, M. Optical Properties of Exfoliated MoS_2 Coaxial Nanotubes—Analogues of Graphene. *Nanoscale Res. Lett.* **2011**, *6*, 593.
243. Deepak, F. L.; Mayoral, A.; Yacaman, M. J. Structural Transformation of MoO_3 Nanobelts into MoS_2 Nanotubes. *Appl. Phys. A: Mater. Sci. Process* **2009**, *96*, 861–867.
244. Seifert, G.; Terrones, H.; Terrones, M.; Jungnickel, G.; Frauenheim, T. Structure and Electronic Properties of MoS_2 Nanotubes. *Phys. Rev. Lett.* **2000**, *85*, 146–149.
245. Lorenz, T.; Teich, D.; Joswig, J.-O.; Seifert, G. Theoretical Study of the Mechanical Behavior of Individual TiS_2 and MoS_2 Nanotubes. *J. Phys. Chem. C* **2012**, *116*, 11714–11721.
246. Remskar, M.; Mrzel, A.; Virsek, M.; Godec, M.; Krause, M.; Kolitsch, A.; Singh, A.; Seabaugh, A. The MoS_2 Nanotubes with Defect-Controlled Electric Properties. *Nanoscale Res. Lett.* **2010**, *6*, 26.
247. Jelenc, J.; Remskar, M. Friction on a Single MoS_2 Nanotube. *Nanoscale Res. Lett.* **2012**, *7*, 208.
248. Mihailovic, D.; Jaglicic, Z.; Arcon, D.; Mrzel, A.; Zorko, A.; Remskar, M.; Kabanov, V. V.; Dominko, R.; Gaberscek, M.; Gomez-Garcia, C. J.; *et al.* Unusual Magnetic State in Lithium-Doped MoS_2 Nanotubes. *Phys. Rev. Lett.* **2003**, *90*, 146401.